

# Grover's algorithm is an approximation of imaginary-time evolution

Yudai Suzuki,<sup>1,2,3</sup> Marek Gluza,<sup>4</sup> Jeongrak Son,<sup>4</sup> Bi Hong Tiang,<sup>4</sup> Nelly H. Y. Ng,<sup>4,5</sup> and Zoë Holmes<sup>1,2</sup>

<sup>1</sup>*Institute of Physics, École Polytechnique Fédérale de Lausanne (EPFL), Lausanne, Switzerland*

<sup>2</sup>*Centre for Quantum Science and Engineering, École Polytechnique Fédérale de Lausanne (EPFL), Lausanne, Switzerland*

<sup>3</sup>*Quantum Computing Center, Keio University, Hiyoshi 3-14-1, Kohoku-ku, Yokohama 223-8522, Japan*

<sup>4</sup>*School of Physical and Mathematical Sciences, Nanyang Technological University, 637371 Singapore*

<sup>5</sup>*Centre for Quantum Technologies, Nanyang Technological University, 50 Nanyang Avenue, 639798 Singapore*

(Dated: September 17, 2025)

We reveal the power of Grover's algorithm from thermodynamic and geometric perspectives by showing that it is a product formula approximation of imaginary-time evolution (ITE), a Riemannian gradient flow on the special unitary group. This viewpoint uncovers three key insights. First, we show that the ITE dynamics trace the shortest path between the initial and the solution states in complex projective space. Second, we prove that the geodesic length of ITE determines the query complexity of Grover's algorithm. This complexity notably aligns with the known optimal scaling for unstructured search. Lastly, utilizing the geodesic structure of ITE, we construct a quantum signal processing formulation for ITE without post-selection, and derive a new set of angles for the fixed-point search. These results collectively establish a deeper understanding of Grover's algorithm and suggest a potential role for thermodynamics and geometry in quantum algorithm design.

## I. INTRODUCTION

Grover's algorithm provides a quadratic speed-up for the unstructured search problem [1], where the goal is to identify marked items within a dataset based on a binary function  $f(x) \in \{0, 1\}$ . Given a search space  $\mathcal{X} \in \{0, 1, \dots, N-1\}$ , the aim is to find  $M$  target items satisfying  $f(x) = 1$ . Classically, solving this problem requires  $\mathcal{O}(N)$  queries, while Grover's algorithm performs the task with only  $\mathcal{O}(\sqrt{N})$  queries [2]. Since unstructured search is a fundamental computational task, the discovery of Grover's algorithm has broadly impacted not only quantum computing, but also various applications such as optimization [3–5], machine learning [6–8], and cryptography [9, 10]. Significant efforts have been devoted to elucidating the characteristics of Grover's algorithm, including its optimal complexity [2, 11–13] and remedies for the “overshooting” issue [14–16]. Grover's framework has been extended to amplitude amplification [17] and further unified under the quantum singular value transformation [18, 19]. These advances underscore Grover's fundamental role in quantum algorithm design.

On the other hand, it is widely observed that, despite decades of research, there are remarkably few quantum algorithmic primitives [20–22]. The search for new primitives is held back, in part, by the difficulty of intuitive unifying understandings of why quantum algorithms work [20]. Uncovering the key factors underlying the success of Grover's algorithm, one of the field's most fundamental primitives, would offer valuable guidance for the principled design of novel, optimal quantum algorithms.

Here, we analyze Grover's algorithm through the lens of Imaginary-Time Evolution (ITE), a thermodynamically-inspired approach to prepare the ground state of a target Hamiltonian. Specifically, we show that the Grover iteration is a product formula approximation of ITE. These ITE dynamics are then equivalent to the steepest descent direc-

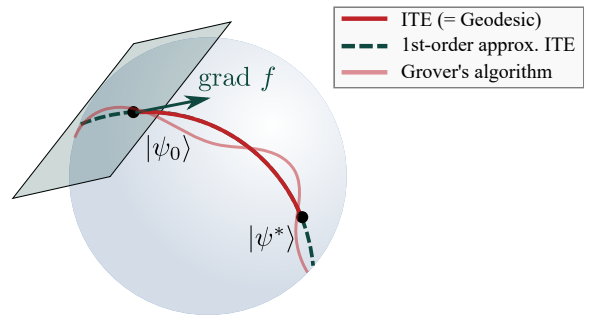


FIG. 1. **Geometrical picture of the unstructured search by Grover's algorithm.** We demonstrate that Grover's algorithm can be viewed as a product formula approximation of Imaginary-Time Evolution (ITE), which corresponds to the steepest descent direction,  $\text{grad } f$ , of a least-squares cost  $f$  on the special unitary group. Moreover, we find that ITE and its first-order approximation of Eq. (7) trace the shortest path (i.e., a geodesic) between the initial state  $|\psi_0\rangle$  and the solution state  $|\psi^*\rangle$ . Accordingly, Grover's algorithm can be understood as a product formula approximation of the geodesic.

tion, i.e., the Riemannian gradient flow, on the special unitary group [23, 24]. Thus we can interpret the success of Grover's algorithm as the implementation of ITE that follows the steepest descent direction on the unitary manifold (see Fig. 1).

Utilizing these findings, we analyze the Grover algorithm's query complexity from a geometric perspective. We first prove that the ITE dynamics trace a geodesic on the complex projective manifold, i.e., the shortest path between the initial and solution states. With this geometric insight, we can express the query complexity of Grover's algorithm in terms of an ITE geodesic length, which recovers the known optimal scaling for unstructured search [2, 11–13]. This result mirrors the framework in Ref. [25], where (in a different context) the optimal synthesis of quantum circuits is cast as a problem of finding a geodesic on a Riemannian manifold. While earlier works have

noted that optimal quantum search can be interpreted in terms of geodesics [26, 27], our work is the first, to our knowledge, to frame Grover's algorithm via ITE, and relate its unitary synthesis to the geodesic length.

Finally, we show that our insights can be used for novel quantum algorithm design. In particular, the findings allow us to prove that the Grover iteration implements quantum signal processing (QSP) [28–31]. We leverage this link to implement ITE without post-selection and a new fixed-point quantum search algorithm. Thus, our findings offer not only a new interpretation of Grover's algorithm, but also potentially provide useful thermodynamic and geometric perspectives that inspire the design of future quantum algorithms.

## II. GROVER'S ALGORITHM AS AN APPROXIMATION OF ITE

We begin by recalling Grover's algorithm. To perform unstructured search, the algorithm first prepares a uniform superposition over all  $N = 2^n$  computational basis states

$$|\psi_0\rangle = \frac{1}{\sqrt{N}} \sum_{x=0}^{N-1} |x\rangle. \quad (1)$$

The algorithm proceeds by repeatedly applying two key operations: the diffusion operator  $D(\alpha) = e^{i\alpha\psi_0}$  and the oracle operator  $U_f(\beta) = e^{i\beta\hat{H}_f}$ , where  $\alpha, \beta \in \mathbb{R}$ ,  $\psi_0 = |\psi_0\rangle\langle\psi_0|$  and

$$\hat{H}_f = \sum_{x \in \{x|f(x)=1\}} |x\rangle\langle x| \quad (2)$$

is the projector onto the subspace of  $M$  marked states. Through  $\mathcal{N}$  repeated applications of  $G_k(\alpha_k, \beta_k) = -D(\alpha_k)U_f(\beta_k)$ , we obtain a final state  $\prod_{k=1}^{\mathcal{N}} G_k(\alpha_k, \beta_k) |\psi_0\rangle$ , that approximates the solution state

$$|\psi^*\rangle = \frac{1}{\sqrt{M}} \sum_{x \in \{x|f(x)=1\}} |x\rangle. \quad (3)$$

The query complexity is then defined as the number of calls  $\mathcal{N}$  to the oracle operator  $U_f$ . The original work in Ref. [1] uses  $\alpha_k = \beta_k = \pi$ , while its variants such as  $\pi/3$ -algorithm [15] and the fixed-point algorithm [16] have been proposed to avoid the so-called soufflé problem [14], where excessive Grover iterations cause the algorithm to overshoot the solution state; see App. A for comprehensive discussions and reviews.

We first show that the unstructured search problem can be solved using Imaginary-Time Evolution (ITE), which drives an initial state to the ground state of the Hamiltonian  $\hat{H}$  via a non-unitary operator  $e^{-\tau\hat{H}}$  with  $\tau \in \mathbb{R}$ . Provided the initial state has non-zero overlap with the ground state, the evolution provably converges to the ground state as  $\tau \rightarrow \infty$  [32]. Similarly, applying ITE with  $\hat{H}_f$  to  $|\psi_0\rangle$  yields the solution state in Eq. (3) in the limit of large  $\tau$ ; see App. C 1 for the proof.

**Lemma 1** (ITE solves the unstructured search problem). *Given the projector Hamiltonian  $\hat{H}_f$  in Eq. (2) and the initial*

*state in Eq. (1), the ITE state converges to the solution state in Eq. (3) as  $\tau \rightarrow \infty$ , i.e.,*

$$\lim_{\tau \rightarrow \infty} \frac{e^{\tau\hat{H}_f} |\psi_0\rangle}{\|e^{\tau\hat{H}_f} |\psi_0\rangle\|_2} = |\psi^*\rangle \quad (4)$$

$$\text{with the normalization factor } \|e^{\tau\hat{H}_f} |\psi_0\rangle\|_2 = \sqrt{\langle\psi_0|e^{2\tau\hat{H}_f}|\psi_0\rangle}.$$

Note that Eq. (4) involves  $e^{\tau\hat{H}_f}$  without a negative sign, as unstructured search seeks the eigenstates of  $\hat{H}_f$  with the largest eigenvalue. Yet, this can also be viewed as the standard ITE, since setting the target Hamiltonian to  $\hat{H}_f \rightarrow -\hat{H}_f$  converts the task into preparing its ground state and introduces a minus sign in the exponents in Eq. (4).

Given Lemma 1, a natural question arises: how can Grover's algorithm be related to ITE for unstructured search? We answer this using the recently-developed framework of Double-Bracket Quantum Algorithms (DBQA) [33], which implements continuous differential equations called double-bracket flows (DBF) [34–51] on quantum computers. Exploiting the equivalence between DBF and ITE (further elaborated in App. B 1), Refs. [33, 52–55] have leveraged the approach to design quantum algorithms that realize ITE.

DBQAs first proceed by recognizing that ITE is a solution to the differential equation

$$\frac{\partial \Psi(\tau)}{\partial \tau} = [[\Psi(\tau), \hat{H}], \Psi(\tau)] \quad (5)$$

with a pure density matrix  $\Psi(\tau) = |\Psi(\tau)\rangle\langle\Psi(\tau)|$  at time  $\tau$ . For arbitrary Hamiltonians  $\hat{H}$ , the discretized solution of Eq. (5) can be approximated to first order as

$$|\psi_s\rangle := e^{s[\hat{H}, \psi_0]} |\psi_0\rangle, \quad (6)$$

where  $s$  is a time duration and  $[A, B] = AB - BA$  is the standard commutator. This approximation generally incurs an error of  $\mathcal{O}(s^2)$  [23, 33, 52, 53]. However, whenever the Hamiltonian is a projector, i.e.,  $\hat{H}^2 = \hat{H}$  as is the case for Grover's algorithm, then the ITE state for any imaginary time  $\tau$  can be realized exactly by Eq. (7) (see App. C 2 for the proof).

**Lemma 2** (Equivalence of ITE and commutator flow for projector Hamiltonians). *Let  $\hat{H}_f$  be the projector Hamiltonian in Eq. (2). Then, for any ITE evolution time  $\tau$ , there exists a time duration  $s_\tau$  such that*

$$\frac{e^{\tau\hat{H}_f} |\psi_0\rangle}{\|e^{\tau\hat{H}_f} |\psi_0\rangle\|_2} = e^{s_\tau[\hat{H}_f, \psi_0]} |\psi_0\rangle = |\psi_{s_\tau}\rangle. \quad (7)$$

*Since the middle expression in Eq. (7) covers all the states generated by ITE, we hereafter refer to  $|\psi_{s_\tau}\rangle$  as the ITE state.*

In the second step of DBQA, the exponential of the commutator in Eq. (7) is approximately implemented using product formula techniques [56–58]. A standard approach is the group commutator

$$e^{s[\hat{H}_f, \psi_0]} = e^{i\sqrt{s}\psi_0} e^{i\sqrt{s}\hat{H}_f} e^{-i\sqrt{s}\psi_0} e^{-i\sqrt{s}\hat{H}_f} + \mathcal{O}(s^{3/2}). \quad (8)$$

Moreover, this can be systematically generalized to higher-order approximations [58]

$$e^{s[\hat{H}_f, \psi_0]} = e^{it_{2N}\psi_0} \dots e^{it_3\hat{H}_f} e^{it_2\psi_0} e^{it_1\hat{H}_f} + \mathcal{O}(s^{m/2}) \quad (9)$$

for certain  $m \in \mathbb{Z}_+$  and  $t_k = c_k\sqrt{s}$  with angles  $\{c_k\}_{k=1}^{2N}$ ; see App. B 2 for specifics in choosing angles. Remarkably, the two exponentials in Eq. (9) are exactly oracle operators  $U_f(t_k)$  and diffusion operators  $D(t_k)$ . In other words, Grover iterations approximate Eq. (7) up to a global phase factor  $(-1)^N$ :

$$\begin{aligned} e^{s[\hat{H}_f, \psi_0]} |\psi_0\rangle &\approx e^{it_{2N}\psi_0} \dots e^{it_3\hat{H}_f} e^{it_2\psi_0} e^{it_1\hat{H}_f} |\psi_0\rangle \\ &= (-1)^N \prod_{k=1}^N G_k(t_{2k}, t_{2k-1}) |\psi_0\rangle. \end{aligned} \quad (10)$$

Therefore, by reformulating unstructured search using ITE, the structure of Grover's algorithm emerges naturally as its approximation via DBQAs.

We note that the overshooting phenomenon in Grover's algorithm can be understood from this derivation. A valuable feature of ITE is its inherent avoidance of overshooting. However, since the first-order approximation in Eq. (7) can generate states that the exact ITE cannot realize (see Fig. 1), the algorithm can also overshoot.

### III. GEODESICS AND ITE DYNAMICS FOR UNSTRUCTURED SEARCH

We exploit the ITE formulation for unstructured search to examine its geometric structure by considering the complex projective space  $\mathbb{CP}^{N-1}$  as a manifold. This space is the set of equivalence classes of non-zero vectors in  $\mathbb{C}^N$ , where  $|\psi\rangle \sim \lambda|\psi\rangle$  for  $\lambda \in \mathbb{C} \setminus \{0\}$ . It naturally arises in quantum mechanics, since pure states are defined only up to a global phase [59]. Equipped with the Fubini–Study metric [59–61], the distance between two normalized states  $|\psi\rangle$  and  $|\phi\rangle$  on the manifold is defined as

$$d_{\text{FS}}(|\psi\rangle, |\phi\rangle) = \arccos(|\langle\psi|\phi\rangle|). \quad (11)$$

The geodesic, which locally minimizes this distance, lies in the two-dimensional subspace spanned by the two states. For instance, given orthonormal states  $|\phi_1\rangle$  and  $|\phi_2\rangle$ , the geodesic is parameterized as  $|\phi(t)\rangle = \cos(t)|\phi_1\rangle + \sin(t)|\phi_2\rangle$ .

With this geometric foundation, we show that the ITE trajectory follows the geodesic. A key step in establishing this result is the construction of a state  $|\psi_0^\perp\rangle$  that is orthogonal to the initial state,  $\langle\psi_0|\psi_0^\perp\rangle = 0$ , defined as

$$|\psi_0^\perp\rangle = \frac{[\hat{H}_f, \psi_0]}{\sqrt{V_0}} |\psi_0\rangle = \frac{\hat{H}_f - E_0 I}{\sqrt{E_0(1 - E_0)}} |\psi_0\rangle, \quad (12)$$

where  $E_0 = \langle\psi_0|\hat{H}_f|\psi_0\rangle = M/N$  and  $V_0 = \langle\psi_0|(\hat{H}_f - E_0)^2|\psi_0\rangle = E_0(1 - E_0)$ . This directly leads to our first main result proven in App. C 3.

**Theorem 3** (ITE traces the geodesic). *Let  $\hat{H}_f$  be the projector in Eq. (2) and  $|\psi_0\rangle$  be the initial state in Eq. (1). Then, the ITE state in Eq. (7) for a time duration  $s$  is*

$$|\psi_s\rangle = \cos(s\sqrt{V_0}) |\psi_0\rangle + \sin(s\sqrt{V_0}) |\psi_0^\perp\rangle. \quad (13)$$

*This traces the geodesic on  $\mathbb{CP}^{N-1}$  connecting the initial state  $|\psi_0\rangle$  to the solution state  $|\psi^*\rangle$ , which is exactly achieved when*

$$s^* = \arccos(\sqrt{E_0})/\sqrt{V_0}. \quad (14)$$

Note that ITE for a general Hamiltonian follows the steepest descent direction with respect to a least-squares cost function [23, 24], whereas geodesics are defined independently of any cost functions. Nevertheless, Theorem 3 shows that, when the Hamiltonian is a projector, the ITE trajectory coincides with the geodesic on  $\mathbb{CP}^{N-1}$ . In App. B 3, we briefly review the relevant geometric structures and explain the connections among the manifold used in the ITE derivation, the special unitary group, and the complex projective space.

### IV. QUERY COMPLEXITY AND GEODESIC LENGTH

Next, we connect the geometric ITE perspective to the query complexity of Grover's algorithm [2, 11–13]. Ref. [25] shows that analyzing geodesics provides a potential framework for understanding the difficulty of implementing quantum algorithms. Specifically, the geodesic length on a Riemannian manifold determines the number of elementary gates required to realize a target unitary operation.

Inspired by Ref. [25], we confirm that the query complexity of Grover's algorithm is determined by the geodesic length of ITE. This link also underlies the ability to achieve the optimal query complexity. This is our second main result, and its proof is provided in App. C 4.

**Theorem 4** (Geodesic length of ITE determines query complexity of Grover's algorithm). *Consider the ITE evolution generated by the operator  $e^{s^*[\hat{H}_f, \psi_0]}$ , such that  $|\psi_{s^*}\rangle = |\psi^*\rangle$  is the solution state from Eq. (14). Then, there exists a Grover iteration  $\prod_{k=1}^N G_k(\alpha_k, \beta_k)$  satisfying*

$$\left\| e^{s^*[\hat{H}_f, \psi_0]} - (-1)^N \prod_{k=1}^N G_k(\alpha_k, \beta_k) \right\|_{\text{op}} \leq \epsilon, \quad (15)$$

*for the operator norm  $\|\cdot\|_{\text{op}}$  and any  $\epsilon \in (0, 2)$ , using the number of queries*

$$\mathcal{N} \in \mathcal{O}\left(\frac{1}{\epsilon^2|\pi/2 - d_{\text{FS}}|}\right) \quad (16)$$

*where  $d_{\text{FS}} \equiv d_{\text{FS}}(|\psi_0\rangle, |\psi^*\rangle)$  is the geodesic length between the initial and solution states, as stated in Eq. (11).*

Theorem 4 shows that the number of queries is determined by the geodesic length. Here, the angles  $\{(\alpha_k, \beta_k)\}_{k=1}^N$  for the Grover iteration are obtained by a simple product formula approximation of ITE. Note that  $d_{\text{FS}}$  ranges over  $[0, \pi/2]$  and

increases with decreasing overlap between the states. This implies that larger distances in the complex projective manifold lead to higher query complexities. Additionally,  $d_{\text{FS}}$  aligns with the geodesic length on the special unitary group equipped with a bi-invariant metric up to a multiplicative factor, and hence a similar result could hold in this setting (see App. C 4).

We further confirm this scaling is optimal in  $N$ , even though the Grover iteration is a simple product formula approximation of ITE. Using the identity  $\pi/2 - \arccos(x) = \arcsin(x)$  and the inequality  $1/\arcsin(x) \leq 1/x$ , we have  $1/|\pi/2 - d_{\text{FS}}| = 1/\arcsin(\sqrt{E_0}) \leq 1/\sqrt{E_0}$ . This also follows from  $|\langle \psi_0 | \psi^* \rangle| = \sqrt{E_0}$ . Since  $E_0 = M/N$ , we get  $1/\sqrt{E_0} \in \mathcal{O}(\sqrt{N})$ . Thus, the query complexity in Theorem 4 scales as  $\sqrt{N}$ , which also matches the known optimality [2].

We remark that our query complexity might not be the best in practice; for instance, Refs. [62, 63] present specific angle sets that could achieve zero error  $\epsilon = 0$  with improved multiplicative factor for  $\sqrt{N}$ . However, our main point is to show that the observation from Ref. [25] can also be applied to unstructured search – i.e., the geodesic length determines the efficiency of the quantum algorithm.

## V. QUANTUM SIGNAL PROCESSING VIA THE GROVER ITERATION FOR ITE AND FIXED-POINT QUANTUM SEARCH

Lastly, we use ITE formulation to shed light on the fixed-point quantum search algorithm [16], which mitigates overshooting while retaining quadratic speed-up. Whereas the original approach determines the required angles using recursive quasi-Chebyshev polynomials [16, 64], our formulation provides an alternative construction by establishing the connection between quantum signal processing (QSP) [28–31] and the Grover iteration.

QSP is a well-established technique for realizing polynomial transformations of a scalar input through interleaved sequences of parameterized unitaries on a two-dimensional subspace. Specifically, given a signal processing operator  $S_Z(\phi) = \text{diag}(e^{i\phi}, e^{-i\phi})$  and a signal operator

$$R(x) = \begin{pmatrix} x & \sqrt{1-x^2} \\ \sqrt{1-x^2} & -x \end{pmatrix}, \quad (17)$$

a QSP sequence applied to  $|0\rangle = (1, 0)^T$ , with an appropriately chosen set of angles  $\{\phi_k\}_{k=0}^K$ , outputs a polynomial

$$p_{QSP}(x) = \langle 0 | S_Z(\phi_K) \prod_{k=0}^{K-1} R(x) S_Z(\phi_k) | 0 \rangle \quad (18)$$

satisfying the conditions in App. B 4. We refer to this construction as  $(R(x), S_Z, |0\rangle)$ -QSP. Since the existence of phases for a wide class of achievable functions in various QSP settings has been rigorously established, QSP underpins many modern quantum algorithms [19, 28–31]; see App. B 4 for details.

We show that Grover iterations implement the  $(R(x), S_Z, |0\rangle)$ -QSP in the two-dimensional subspace spanned by the initial and the solution states. Most previous studies including Refs. [2, 16, 64] consider a subspace spanned by  $\{|\psi^*\rangle, |\psi_\perp^*\rangle\}$

with  $|\psi_\perp^*\rangle = (\hat{H}_f - I) |\psi_0\rangle / \sqrt{1 - E_0}$ . We instead adopt the basis  $\{|\psi_0\rangle, |\psi_0^\perp\rangle\}$  introduced in Theorem 3. In this basis, the diffusion and oracle operations take the form

$$D(\alpha) = e^{i\alpha\psi_0} = e^{i\alpha/2} S_Z(\alpha/2) \quad (19)$$

$$U_f(\beta) = e^{i\beta\hat{H}_f} = e^{i\beta/2} R(\sqrt{E_0}) S_Z(\beta/2) R(\sqrt{E_0}), \quad (20)$$

respectively. This leads to Theorem 5 proven in Appendix C 5.

**Theorem 5** (Grover iteration realizes a QSP sequence). *Given the basis  $\{|\psi_0\rangle, |\psi_0^\perp\rangle\}$  corresponding to  $\{|0\rangle, |1\rangle\}$ , the Grover iteration  $\prod_{k=1}^N G_k(\alpha_k, \beta_k) |\psi_0\rangle$  executes the  $(R(\sqrt{E_0}), S_Z, |0\rangle)$ -QSP of Eq. (18) for  $K = 2N$ , i.e.,*

$$\prod_{k=1}^N G_k(\alpha_k, \beta_k) |\psi_0\rangle = S_Z(\phi_{2N}) \prod_{k=0}^{2N-1} R(\sqrt{E_0}) S_Z(\phi_k) |0\rangle, \quad (21)$$

where  $\phi_0 = N\pi + \sum_{l=1}^N (\alpha_l + \beta_l)/2$ ,  $\phi_{2l-1} = \beta_l/2$  and  $\phi_{2l} = \alpha_l/2$  for  $l = 1, \dots, N$ .

In the  $\{|\psi_0\rangle, |\psi_0^\perp\rangle\}$  basis, the ITE state in Eq. (13) takes the simple form

$$|\psi_s\rangle = \begin{pmatrix} \cos(s\sqrt{V_0}) \\ \sin(s\sqrt{V_0}) \end{pmatrix} \quad (22)$$

with  $V_0 = E_0(1 - E_0)$ . It then follows from Theorem 5 that, if the function  $\cos(sx\sqrt{1-x^2})$  can be realized by  $(R(x), S_Z, |0\rangle)$ -QSP, then the ITE state, Eq. (22), can be realized *without prior knowledge of  $E_0$* . This is because the task reduces to tailoring QSP angles that approximate the desired polynomial. We show in App. C 5 that the target function meets the achievability conditions by the QSP convention. Thus the Jacobi–Anger expansion, which has been exploited for the efficient construction of trigonometric functions in the QSP community [18, 19], can be utilized. Therefore, for sufficiently large  $N$ , QSP may approximate the ITE state effectively.

We further use Theorem 5 to derive a new set of angles for a fixed-point algorithm. Concretely, we realize the solution state without information on  $E_0$ , even though the optimal time duration  $s^*$  in Eq. (14) depends on it. We note that applying  $R(\sqrt{E_0})$  to the initial state directly prepares the solution state  $|\psi^*\rangle = (\sqrt{E_0}, \sqrt{1 - E_0})^T$ . However, we cannot apply a single signal operator alone with the Grover iterations, as the oracle consists of  $K = 2N$  signal operators. Yet, if we find QSP sequence  $W$  of length  $K = 2N - 1$  such that  $W|0\rangle = |0\rangle$ , the Grover iteration with  $N$  (i.e.,  $K = 2N$  in the QSP convention)

$$\prod_{k=1}^N G_k(\alpha_k, \beta_k) |\psi_0\rangle = S_Z(\phi_{2N}) R(\sqrt{E_0}) W |0\rangle \quad (23)$$

can prepare  $|\psi^*\rangle$  by setting  $\phi_{2N} = 0$ .

The remaining step is to identify a function that QSP can implement to realize  $W|0\rangle = |0\rangle$ . The key requirement is  $p_{QSP}(\sqrt{E_0}) = \langle 0 | W | 0 \rangle = 1$ , while the values of  $p_{QSP}(x)$  for negative  $x$  are irrelevant since  $\sqrt{E_0}$  is always positive. Also, as  $W$  involves an odd number ( $2N - 1$ ) of applications of the signal operator, the function  $p_{QSP}(x)$  must be odd.

A natural choice is the sign function and hence we consider  $p_{QSP}(x) = \text{sgn}(x)$ .

The sign function can be efficiently approximated via a polynomial function of degree  $d \in \mathcal{O}(1/\sqrt{E_0} \log(1/\epsilon))$  with error  $\epsilon$  and thus this approach achieves the optimal scaling in  $N$  (see App. C 5). However, the sign function does not satisfy the conditions for achievable functions by  $(R(x), S_Z, |0\rangle)$ -QSP. Nevertheless, Ref. [19] shows that introducing a small imaginary part into the QSP phases allows the sign function to be approximated. Although this might sacrifice the optimal scaling with  $N$  as shown in App. D, we obtain a scaling similar to the standard fixed-point Grover algorithm.

## VI. DISCUSSION

In the comment piece titled “*Why haven’t more quantum algorithms been found?*” [20], P. Shor argued “quantum computers operate in a manner so different from classical computers that our techniques for designing algorithms and our intuitions for understanding the process of computation no longer work”. Here, however, we show that Grover’s algorithm can be viewed through the well-established lenses of Riemannian optimization and ITE. Namely, Grover’s algorithm simply performs Riemannian optimization, a standard classical optimization strategy, but on the manifold of unitaries.

In this manner, our results highlight the role of geometric analysis in quantum algorithm design. Theorem 3 demonstrates that knowledge of the geodesic enables a dimensionality reduction, which potentially simplifies the design and analysis of other quantum algorithms. Moreover, Theorem 4 confirms that the query complexity associated with the geodesic length achieves the known optimal scaling in unstructured search. These findings reinforce the significance of geometry-inspired approaches in developing quantum algorithms, advo-

cated in Ref. [25]. While determining geodesics may be challenging in general and ITE paths do not always coincide with geodesics, our results underscore their relevance for the design and analysis of quantum algorithms via the geometry. Finally, Theorem 5 shows how these geometric observations can be used to design a new fixed-point quantum search algorithm.

While the optimal query complexity for unstructured search is limited to a quadratic speed-up, ITE in general converges exponentially in  $\tau$  to the target state. This seeming tension could stem from the first-order approximation used to derive the Grover iteration from ITE. Exploring this difference could clarify the fundamental cost of realizing thermodynamically-inspired approaches in a fully unitary framework. Specifically, given the optimality of Grover’s algorithm, it may suggest that implementing ITE through real-time (unitary) evolution may benefit a quadratic advantage at best. Conversely, this gap could motivate the development of novel quantum algorithms that incorporate non-unitary operations directly.

This work clarifies the power of Grover’s algorithm by showing that it naturally emerges from an approximation of ITE. A natural direction for future work is to extend this perspective to a broader class of quantum algorithms. For amplitude amplification [17] where the target is a pure state (i.e., a projector), our ITE-based analysis may be directly applicable. However, analyzing its variants such as oblivious amplitude amplification [65] could be non-trivial. Exploring whether the ITE framework reveals mechanisms behind the success of such algorithms may provide more valuable insights into the search for quantum advantage.

*Acknowledgments.* ZH acknowledges support from the Sandoz Family Foundation-Monique de Meuron program for Academic Promotion. MG, JS, BH and NN are supported by the start-up grant of the Nanyang Assistant Professorship at the Nanyang Technological University in Singapore.

---

[1] Grover, L. K. A fast quantum mechanical algorithm for database search. In *Proceedings of the twenty-eighth annual ACM symposium on Theory of computing*, 212–219 (1996). URL <https://doi.org/10.1145/237814.237866>.

[2] Nielsen, M. A. & Chuang, I. L. *Quantum computation and quantum information* (Cambridge university press, 2010). URL <https://dl.acm.org/doi/10.5555/1972505>.

[3] Durr, C. & Hoyer, P. A quantum algorithm for finding the minimum. *arXiv preprint quant-ph/9607014* (1996). URL <https://arxiv.org/abs/quant-ph/9607014>.

[4] Gilliam, A., Woerner, S. & Gonciulea, C. Grover adaptive search for constrained polynomial binary optimization. *Quantum* **5**, 428 (2021). URL <https://doi.org/10.22331/q-2021-04-08-428>.

[5] Baritompa, W. P., Bulger, D. W. & Wood, G. R. Grover’s quantum algorithm applied to global optimization. *SIAM Journal on Optimization* **15**, 1170–1184 (2005). URL <https://doi.org/10.1137/040605072>.

[6] Dong, D., Chen, C., Li, H. & Tarn, T.-J. Quantum reinforcement learning. *IEEE Transactions on Systems, Man, and Cybernetics, Part B (Cybernetics)* **38**, 1207–1220 (2008). URL <https://dl.acm.org/doi/abs/10.1109/TSMCB.2008.925743>.

[7] Du, Y., Hsieh, M.-H., Liu, T. & Tao, D. A Grover-search based quantum learning scheme for classification. *New Journal of Physics* **23**, 023020 (2021). URL <https://iopscience.iop.org/article/10.1088/1367-2630/abdefa>.

[8] Muser, T., Zapusek, E., Belis, V. & Reiter, F. Provable advantages of kernel-based quantum learners and quantum preprocessing based on Grover’s algorithm. *Physical Review A* **110**, 032434 (2024). URL <https://doi.org/10.1103/PhysRevA.110.032434>.

[9] Brassard, G., Høyer, P. & Tapp, A. Quantum cryptanalysis of hash and claw-free functions. In *LATIN’98: Theoretical Informatics: Third Latin American Symposium Campinas, Brazil, April 20–24, 1998 Proceedings* 3, 163–169 (Springer, 1998). URL <https://doi.org/10.1145/261342.261346>.

[10] Bernstein, D. J. Cost analysis of hash collisions: Will quantum computers make SHARCS obsolete. *SHARCS* **9**, 105 (2009). URL <http://cr.yp.to/hash/collisioncost-20090823.pdf>.

[11] Bennett, C. H., Bernstein, E., Brassard, G. & Vazirani, U. Strengths and weaknesses of quantum computing. *SIAM journal on Computing* **26**, 1510–1523 (1997). URL <https://doi.org/10.1137/S0097539795281775>.

[org/10.1137/S0097539796300933](https://doi.org/10.1137/S0097539796300933).

[12] Beals, R., Buhrman, H., Cleve, R., Mosca, M. & de Wolf, R. Tight quantum bounds by polynomials. In *Proceedings of the Thirty-ninth Annual Symposium on Foundations of Computer Science (FOCS)* (Citeseer, 1998). URL <https://doi.org/10.1145/3188745.3188784>.

[13] Zalka, C. Grover's quantum searching algorithm is optimal. *Physical Review A* **60**, 2746 (1999). URL <https://doi.org/10.1103/PhysRevA.60.2746>.

[14] Brassard, G. Searching a quantum phone book. *Science* **275**, 627–628 (1997). URL <https://doi.org/10.1126/science.275.5300.627>.

[15] Grover, L. K. Fixed-point quantum search. *Physical Review Letters* **95**, 150501 (2005). URL <https://doi.org/10.1103/PhysRevLett.95.150501>.

[16] Yoder, T. J., Low, G. H. & Chuang, I. L. Fixed-point quantum search with an optimal number of queries. *Physical Review Letters* **113**, 210501 (2014). URL <https://doi.org/10.1103/PhysRevLett.113.210501>.

[17] Brassard, G., Hoyer, P., Mosca, M. & Tapp, A. Quantum amplitude amplification and estimation. *Contemporary Mathematics* **305**, 53–74 (2002). URL <https://doi.org/10.1090/conm/305/05215>.

[18] Gilyén, A., Su, Y., Low, G. H. & Wiebe, N. Quantum singular value transformation and beyond: exponential improvements for quantum matrix arithmetics. In *Proceedings of the 51st Annual ACM SIGACT Symposium on Theory of Computing*, 193–204 (2019). URL <https://dl.acm.org/doi/abs/10.1145/3313276.3316366>.

[19] Martyn, J. M., Rossi, Z. M., Tan, A. K. & Chuang, I. L. Grand unification of quantum algorithms. *PRX Quantum* **2**, 040203 (2021). URL <https://link.aps.org/doi/10.1103/PRXQuantum.2.040203>.

[20] Shor, P. W. Why haven't more quantum algorithms been found? *Journal of the ACM (JACM)* **50**, 87–90 (2003). URL <https://doi.org/10.1145/602382.602408>.

[21] Zimborás, Z. *et al.* Myths around quantum computation before full fault tolerance: What no-go theorems rule out and what they don't. *arXiv preprint arXiv:2501.05694* (2025). URL <https://arxiv.org/abs/2501.05694>.

[22] Dalzell, A. M. *et al.* Quantum algorithms: A survey of applications and end-to-end complexities. *arXiv preprint arXiv:2310.03011* (2023). URL <https://doi.org/10.1017/9781009639651>.

[23] Gluza, M. *et al.* Double-bracket quantum algorithms for quantum imaginary-time evolution. *arXiv preprint arXiv:2412.04554* (2024). URL <https://arxiv.org/abs/2412.04554>.

[24] McMahon, N. A., Pervez, M. & Arenz, C. Equating quantum imaginary time evolution, riemannian gradient flows, and stochastic implementations. *arXiv preprint arXiv:2504.06123* (2025). URL <https://doi.org/10.48550/arXiv.2504.06123>.

[25] Nielsen, M. A., Dowling, M. R., Gu, M. & Doherty, A. C. Quantum computation as geometry. *Science* **311**, 1133–1135 (2006). URL <https://doi.org/10.1126/science.1121541>.

[26] Miyake, A. & Wadati, M. Geometric strategy for the optimal quantum search. *Physical Review A* **64**, 042317 (2001). URL <https://doi.org/10.1103/PhysRevA.64.042317>.

[27] Cafaro, C. & Mancini, S. On Grover's search algorithm from a quantum information geometry viewpoint. *Physica A: Statistical Mechanics and its Applications* **391**, 1610–1625 (2012). URL <https://doi.org/10.1016/j.physa.2011.09.018>.

[28] Low, G. H. *Quantum signal processing by single-qubit dynamics*. Ph.D. thesis, Massachusetts Institute of Technology (2017). URL <http://hdl.handle.net/1721.1/115025>.

[29] Low, G. H. & Chuang, I. L. Optimal Hamiltonian simulation by quantum signal processing. *Physical Review Letters* **118**, 010501 (2017). URL <https://doi.org/10.1103/PhysRevLett.118.010501>.

[30] Low, G. H., Yoder, T. J. & Chuang, I. L. Methodology of resonant equiangular composite quantum gates. *Phys. Rev. X* **6**, 041067 (2016). URL <https://link.aps.org/doi/10.1103/PhysRevX.6.041067>.

[31] Motlagh, D. & Wiebe, N. Generalized quantum signal processing. *PRX Quantum* **5**, 020368 (2024). URL <https://doi.org/10.1103/PRXQuantum.5.020368>.

[32] Gell-Mann, M. & Low, F. Bound states in quantum field theory. *Phys. Rev.* **84**, 350–354 (1951). URL <https://link.aps.org/doi/10.1103/PhysRev.84.350>.

[33] Gluza, M. Double-bracket quantum algorithms for diagonalization. *Quantum* **8**, 1316 (2024). URL <https://doi.org/10.22331/q-2024-04-09-1316>.

[34] Bloch, A. M. A completely integrable Hamiltonian system associated with line fitting in complex vector spaces. *Bull. Amer. Math. Soc.* (1985). URL <https://doi.org/10.1090/S0273-0979-1985-15365-0>.

[35] Bloch, A. M. Steepest descent, linear programming and Hamiltonian flows. *Contemp. Math. AMS* **114**, 77–88 (1990). URL <https://doi.org/10.1090/conm/114>.

[36] Bloch, A. M., Brockett, R. W. & Ratiu, T. S. Completely integrable gradient flows. *Communications in Mathematical Physics* **147**, 57–74 (1992). URL <https://doi.org/10.1007/BF02099528>.

[37] Brockett, R. Dynamical systems that sort lists, diagonalize matrices, and solve linear programming problems. *Linear Algebra and its Applications* **146**, 79–91 (1991). URL [https://doi.org/10.1016/0024-3795\(91\)90021-N](https://doi.org/10.1016/0024-3795(91)90021-N).

[38] Bloch, A. Estimation, principal components and hamiltonian systems. *Systems & Control Letters* **6**, 103–108 (1985). URL <https://www.sciencedirect.com/science/article/pii/0167691185900052>.

[39] Moore, J., Mahony, R. & Helmke, U. Numerical gradient algorithms for eigenvalue and singular value calculations. *SIAM Journal on Matrix Analysis and Applications* **15**, 881–902 (1994). URL <https://doi.org/10.1137/S0036141092229732>.

[40] Brockett, R. Least squares matching problems. *Linear Algebra and its Applications* **122-124**, 761–777 (1989). URL <https://www.sciencedirect.com/science/article/pii/0024379589906757>. Special Issue on Linear Systems and Control.

[41] Deift, P., Nanda, T. & Tomei, C. Ordinary differential equations and the symmetric eigenvalue problem. *SIAM Journal on Numerical Analysis* **20**, 1–22 (1983). URL <https://doi.org/10.1137/0720001>.

[42] Chu, M. T. On the continuous realization of iterative processes. *SIAM Review* **30**, 375–387 (1988). URL <http://www.jstor.org/stable/2030697>.

[43] Wegner, F. Flow-equations for Hamiltonians. *Annalen der physik* **506**, 77–91 (1994). URL <https://doi.org/10.1002/andp.19945060203>.

[44] Wegner, F. Flow equations and normal ordering: a survey. *Journal of Physics A: Mathematical and General* **39**, 8221 (2006). URL <https://doi.org/10.1088/0305-4470/39/33/003>.

0305-4470/39/25/S29.

[45] Hastings, M. B. On Lieb-Robinson Bounds for the Double Bracket Flow (2022). URL <https://arxiv.org/abs/2201.07141>. 2201.07141.

[46] Glazek, S. D. & Wilson, K. G. Renormalization of Hamiltonians. *Phys. Rev. D* **48**, 5863–5872 (1993). URL <https://link.aps.org/doi/10.1103/PhysRevD.48.5863>.

[47] Glazek, S. D. & Wilson, K. G. Perturbative renormalization group for Hamiltonians. *Phys. Rev. D* **49**, 4214–4218 (1994). URL <https://link.aps.org/doi/10.1103/PhysRevD.49.4214>.

[48] Kehrein, S. The flow equation approach to many-particle systems. *Springer Tracts Mod. Phys.* **217**, 1–170 (2006). URL <https://doi.org/10.1007/3-540-34068-8>.

[49] Smith, S. T. *Geometric optimization methods for adaptive filtering* (Harvard University, 1993). URL <https://doi.org/10.48550/arXiv.1305.1886>.

[50] Helmke, U. & Moore, J. B. *Optimization and dynamical systems* (Springer Science & Business Media, 2012). URL <https://link.springer.com/book/10.1007/978-1-4471-3467-1>.

[51] Brockett, R. W. Smooth dynamical systems which realize arithmetical and logical operations. *Three Decades of Mathematical System Theory: A Collection of Surveys at the Occasion of the 50th Birthday of Jan C. Willems* 19–30 (2005). URL <https://doi.org/10.1007/BFb0008457>.

[52] Robbiati, M. *et al.* Double-bracket quantum algorithms for high-fidelity ground state preparation (2024). URL <https://arxiv.org/abs/2408.03987>.

[53] Xiaoyue, L. *et al.* Strategies for optimizing double-bracket quantum algorithms. *arXiv preprint arXiv:2408.07431* (2024). URL <https://doi.org/10.48550/arXiv.2408.07431>.

[54] Zander, R., Seidel, R., Xiaoyue, L. & Gluza, M. Role of Riemannian geometry in double-bracket quantum imaginary-time evolution. *arXiv preprint arXiv:2504.01065* (2025). URL <https://doi.org/10.48550/arXiv.2504.01065>.

[55] Suzuki, Y. *et al.* Double-bracket algorithm for quantum signal processing without post-selection. *arXiv preprint arXiv:2504.01077* (2025). URL <https://doi.org/10.48550/arXiv.2504.01077>.

[56] Dawson, C. M. & Nielsen, M. A. The Solovay-Kitaev algorithm. *Quantum Information & Computation* **6**, 81–95 (2006). URL <https://dl.acm.org/doi/abs/10.5555/2011679.2011685>.

[57] Chen, Y.-A. *et al.* Efficient product formulas for commutators and applications to quantum simulation. *Phys. Rev. Res.* **4**, 013191 (2022). URL <https://doi.org/10.1103/PhysRevResearch.4.013191>.

[58] Childs, A. M. & Wiebe, N. Product formulas for exponentials of commutators. *Journal of Mathematical Physics* **54** (2013). URL <https://doi.org/10.1063/1.4811386>.

[59] Bengtsson, I. & Życzkowski, K. *Geometry of quantum states: an introduction to quantum entanglement* (Cambridge university press, 2017). URL <https://doi.org/10.1017/CBO9780511535048>.

[60] Anandan, J. & Aharonov, Y. Geometry of quantum evolution. *Physical Review Letters* **65**, 1697 (1990). URL <https://doi.org/10.1103/PhysRevLett.65.1697>.

[61] Mukunda, N. & Simon, R. Quantum kinematic approach to the geometric phase. I. General formalism. *Annals of Physics* **228**, 205–268 (1993). URL <https://doi.org/10.1006/aphy.1993.1093>.

[62] Long, G. L. Grover algorithm with zero theoretical failure rate. *Phys. Rev. A* **64**, 022307 (2001). URL <https://link.aps.org/doi/10.1103/PhysRevA.64.022307>.

[63] Roy, T., Jiang, L. & Schuster, D. I. Deterministic grover search with a restricted oracle. *Phys. Rev. Res.* **4**, L022013 (2022). URL <https://link.aps.org/doi/10.1103/PhysRevResearch.4.L022013>.

[64] Li, G. & Li, L. Revisiting fixed-point quantum search: proof of the quasi-Chebyshev lemma. *arXiv preprint arXiv:2403.02057* (2024). URL <https://doi.org/10.48550/arXiv.2403.02057>.

[65] Berry, D. W., Childs, A. M., Cleve, R., Kothari, R. & Somma, R. D. Exponential improvement in precision for simulating sparse Hamiltonians. In *Proceedings of the forty-sixth annual ACM symposium on Theory of computing*, 283–292 (2014). URL <https://dl.acm.org/doi/10.1145/2591796.2591854>.

[66] Grover, L. K. From Schrödinger’s equation to the quantum search algorithm. *American Journal of Physics* **69**, 769–777 (2001). URL <https://doi.org/10.1007/s12043-001-0128-3>.

[67] Farhi, E. & Gutmann, S. Analog analogue of a digital quantum computation. *Physical Review A* **57**, 2403 (1998). URL <https://doi.org/10.1103/PhysRevA.57.2403>.

[68] Lin, C., Wang, Y., Kolesov, G. & Kalabić, U. Application of Pontryagin’s minimum principle to Grover’s quantum search problem. *Physical Review A* **100**, 022327 (2019). URL <https://doi.org/10.1103/PhysRevA.100.022327>.

[69] Carlini, A., Hosoya, A., Koike, T. & Okudaira, Y. Time-optimal quantum evolution. *Physical Review Letters* **96**, 060503 (2006). URL <https://doi.org/10.1103/PhysRevLett.96.060503>.

[70] Grover, L. K. & Sengupta, A. M. Classical analog of quantum search. *Physical Review A* **65**, 032319 (2002). URL <https://doi.org/10.1103/PhysRevA.65.032319>.

[71] Wiersema, R. & Killoran, N. Optimizing quantum circuits with Riemannian gradient flow. *Phys. Rev. A* **107**, 062421 (2023). URL <https://link.aps.org/doi/10.1103/PhysRevA.107.062421>.

[72] Kuperberg, G. Breaking the cubic barrier in the Solovay-Kitaev algorithm. *arXiv preprint arXiv:2306.13158* (2023). URL <https://doi.org/10.48550/arXiv.2306.13158>.

[73] Elkasapy, A. & Thom, A. On the length of the shortest non-trivial element in the derived and the lower central series. *Journal of Group Theory* **18**, 793–804 (2015). URL <https://doi.org/10.1515/jgth-2015-0007>.

[74] Elkasapy, A. A new construction for the shortest non-trivial element in the lower central series. *arXiv preprint arXiv:1610.09725* (2016). URL <https://doi.org/10.48550/arXiv.1610.09725>.

[75] Peetz, J. & Narang, P. Hamiltonian Simulation via Stochastic Zassenhaus Expansions. *arXiv preprint arXiv:2501.13922* (2025). URL <https://doi.org/10.48550/arXiv.2501.13922>.

[76] Kobayashi, S. & Nomizu, K. *Foundations of differential geometry, volume 2*, vol. 2 (John Wiley & Sons, 1996).

[77] Lewis, D., Wiersema, R., Carrasquilla, J. & Bose, S. Geodesic algorithm for unitary gate design with time-independent Hamiltonians. *Physical Review A* **111**, 052618 (2025). URL <https://doi.org/10.1103/PhysRevA.111.052618>.

[78] Lin, L. & Tong, Y. Near-optimal ground state preparation. *Quantum* **4**, 372 (2020). URL <https://doi.org/10.22331/q-2020-12-14-372>.

[79] Virtanen, P. *et al.* SciPy 1.0: Fundamental Algorithms for Scientific Computing in Python. *Nature Methods* **17**,

261–272 (2020). URL <https://doi.org/10.1038/s41592-019-0686-2>.

# Appendix

## Table of Contents

---

<b>A</b>	<b>A quick overview of Grover's algorithm</b>	<b>10</b>
<b>B</b>	<b>Preliminaries</b>	<b>11</b>
1	Interplay between double-bracket flow, Riemannian gradient flow and ITE . . . . .	11
2	Review of product formula for commutators . . . . .	13
3	Overview on Geometry of Manifolds . . . . .	15
4	Overview of Quantum Signal Processing . . . . .	16
<b>C</b>	<b>Proofs in the Main Texts</b>	<b>17</b>
1	Proof of Lemma 1 . . . . .	17
2	Proof of Lemma 2 . . . . .	18
3	Proof of Theorem 3 . . . . .	19
4	Proof of Theorem 4 . . . . .	20
5	Proof of Theorem 5 . . . . .	23
<b>D</b>	<b>Numerical Simulations</b>	<b>26</b>

---

## Appendix A: A quick overview of Grover's algorithm

We begin by briefly reviewing the setup of Grover's algorithm. Given a search space  $\mathcal{X} \in \{0, 1, \dots, N-1\}$ , the goal of unstructured search is to identify  $M$  target items for which a binary function  $f(x) \in \{0, 1\}$  satisfies  $f(x) = 1$ . The algorithm starts by preparing a uniform superposition over all  $N = 2^n$  computational basis states by applying the Hadamard gate  $H$  to each of the  $n$  qubits;

$$|\psi_0\rangle = H^{\otimes n} |0^{\otimes n}\rangle = \frac{1}{\sqrt{N}} \sum_{x=0}^{N-1} |x\rangle. \quad (\text{A1})$$

The algorithm then proceeds by repeatedly applying two key operations: the diffusion operator  $D(\alpha)$  and the oracle operator  $U_f(\beta)$  with  $\alpha, \beta \in \mathbb{R}$  defined as

$$U_f(\beta) = e^{i\beta\hat{H}_f} = I - (1 - e^{i\beta})\hat{H}_f, \quad (\text{A2})$$

$$D(\alpha) = e^{i\alpha\psi_0} = I - (1 - e^{i\alpha})\psi_0, \quad (\text{A3})$$

respectively. Here,  $\psi_0 = |\psi_0\rangle\langle\psi_0|$  and

$$\hat{H}_f = \sum_{x \in \{x|f(x)=1\}} |x\rangle\langle x| \quad (\text{A4})$$

is the projector onto the subspace of  $M$  marked states. Through  $\mathcal{N}$  repeated applications of  $G_k(\alpha_k, \beta_k) = -D(\alpha_k)U_f(\beta_k)$  to the initial state, we obtain a final state  $\prod_{k=1}^{\mathcal{N}} G_k(\alpha_k, \beta_k) |\psi_0\rangle$ , which is intended to approximate the solution state

$$|\psi^*\rangle = \frac{1}{\sqrt{M}} \sum_{x \in \{x|f(x)=1\}} |x\rangle. \quad (\text{A5})$$

The original work in Ref. [1] uses  $\alpha_k = \beta_k = \pi$  and shows that the query complexity defined as the number of calls  $\mathcal{N}$  to the oracle operator  $U_f$  is optimal [2].

Following the introduction of Grover's algorithm [1], numerous works have attempted to characterize its computational capabilities. A key line of research has rigorously established its asymptotic optimality in terms of query complexity [2, 11–13]. In parallel, other work has addressed the so-called soufflé problem [14], in which repeated applications of Grover's iteration can overshoot the optimal solution; this makes it difficult to determine the correct number of iterations without prior knowledge of the number of marked items. The  $\pi/3$ -algorithm [15], where the angles are set to

$$\alpha_k = \beta_k = \frac{\pi}{3}, \quad (\text{A6})$$

mitigates overshooting but sacrifices the optimal quadratic speed-up. To overcome this trade-off, the fixed-point search algorithm was introduced to alleviate overshooting while retaining optimal query complexity [16]. The key point of the fixed-point algorithm is to utilize recursive quasi-Chebyshev polynomials [16, 64] for generating phase angles that guarantee monotonic convergence; the angles are given by

$$\alpha_k = \beta_{\mathcal{N}-k+1} = -\cot^{-1} \left( \tan \left( \frac{2\pi k}{\mathcal{N}} \right) \sqrt{1 - \frac{1}{\gamma^2}} \right), \quad (\text{A7})$$

where  $\gamma = T_{1/\mathcal{N}}(1/\delta)$  with the Chebyshev polynomials of the first kind  $T_d(\cdot)$  of the degree  $d$  for a desired precision of the final fidelity, that is,  $F \geq 1 - \delta^2$ . This approach is especially practical, as it ensures reliable performance without requiring prior knowledge of the initial overlap, provided the overlap exceeds a certain threshold. The aforementioned algorithms generally do not guarantee unit success probability, Refs. [62, 63] present deterministic approaches to the solution, i.e., algorithms with phase angles that achieve zero error in the final state.

There have also been efforts to understand the power of Grover's algorithm in terms of its geometric structure [26, 27]. Ref. [26] considers the complex projective space to investigate the entanglement through the Grover's algorithm, while Ref. [27] introduces Wigner-Yanase quantum information metric to recast the unstructured search task in the framework of information geometry.

Previous studies have also explored quantum search algorithms from the perspective of Hamiltonian simulation [2, 66–69]. For instance, it has been shown that real-time evolution  $e^{it\tilde{H}}$  under the Hamiltonian  $\tilde{H} = |\psi^*\rangle\langle\psi^*| + |\psi_0\rangle\langle\psi_0|$  can drive the initial state  $|\psi_0\rangle$  toward the target solution state  $|\psi^*\rangle$ . We emphasize that, while these results represent important early attempts to understand unstructured search in terms of Hamiltonian dynamics, they do not provide a clear explanation for the origin of

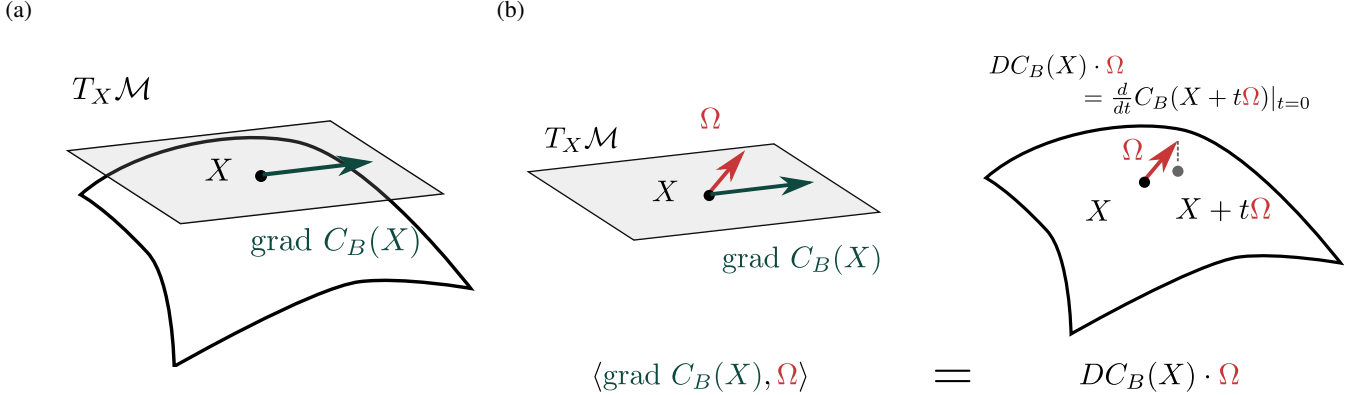


FIG. 2. **Two conditions that characterize the Riemannian gradient.** The Riemannian gradient is uniquely characterized by two conditions: (a) the tangency condition and (b) the compatibility condition.

Grover's circuit structure or its connection to ITE, as established in our results. In addition, classical analogs have been explored to further investigate the power of quantum search algorithms [70].

Beyond this, the conceptual framework of Grover's algorithm has also been generalized to amplitude amplification [17], a fundamental technique that underpins many advanced quantum algorithms. This broader framework is further unified by the quantum singular value transformation formalism [18, 19]. As such, the principles underlying Grover's algorithm form a cornerstone of modern quantum algorithm design. This indicates that understanding its mathematical structure plays a core role in both advancing theoretical insights and guiding the practical development of quantum algorithms.

## Appendix B: Preliminaries

### 1. Interplay between double-bracket flow, Riemannian gradient flow and ITE

We give an overview showing that the dynamics of imaginary-time evolution (ITE) corresponds to the steepest descent direction of a least-squares cost function defined on a Riemannian manifold. To establish this, we proceed in two steps. First, we demonstrate that the double-bracket flow (DBF) [34–51] characterizes the Riemannian gradient flow of a least-squares cost function. Second, we show that ITE naturally takes the form of a DBF.

We begin with a brief overview of DBF. In general, DBFs are matrix-valued ordinary differential equations that have been employed to perform matrix diagonalization, QR decomposition, eigenvalue sorting, and related tasks [37, 41, 42, 50]. Brockett originally introduced this flow in the context of minimizing a least-squares cost between two matrices using steepest descent techniques. Consider the set of matrices

$$\mathcal{M}(A) = \{U A U^\dagger \text{ s.t. } U^{-1} = U^\dagger\} \quad (\text{B1})$$

generated by unitary evolution of a Hermitian operator  $A$  and the least-squares cost  $C_{A,B}(U) = -\frac{1}{2}\|U A U^\dagger - B\|_{\text{HS}}^2$  with a Hermitian  $B$  and the Hilbert-Schmidt norm  $\|\cdot\|_{\text{HS}}$ . Let  $X = U A U^\dagger$  be a point on the manifold  $\mathcal{M}(A)$  and define the cost as

$$C_B(X) = -\frac{1}{2}\|X - B\|_{\text{HS}}^2. \quad (\text{B2})$$

Then, the Riemannian gradient of the cost  $C_B$  at  $X$  is given by [50, 71]

$$\text{grad}_X C_B(X) = [[X, B], X]. \quad (\text{B3})$$

We note that the matrix  $B$  should be chosen properly depending on the task at hand. For example, if  $B$  is a diagonal matrix with entries  $\text{diag}(1, 2, 3, \dots)$ , then the DBF in Eq. (B3) drives the matrix  $X$  towards a diagonal matrix whose entries are the eigenvalues of  $X$  sorted in ascending order [37]. By varying the diagonal entries of  $B$ , the order in which the eigenvalues appear in the diagonalized form of  $X$  can be controlled. See Refs. [34–51] for other applications of DBF.

Now, we elaborate on how Eq. (B3) is derived. A key point of the derivation is two properties that uniquely characterize the Riemannian gradient on manifolds:

- **Tangency condition:** the Riemannian gradient of a smooth function  $C_B$  at point  $X \in \mathcal{M}(A)$  lies in the tangent space  $T_X \mathcal{M}(A)$  of the manifold  $\mathcal{M}(A)$ ,

$$\text{grad } C_B(X) \in T_X \mathcal{M}(A), \forall X \in \mathcal{M}(A).$$

This property guarantees that the Riemannian gradient must be an element of the tangent space  $T_X \mathcal{M}(A)$  of the manifold.

- **Compatibility condition:** given the differential  $DC_B \in \cup_{X \in \mathcal{M}(A)} T_X^* \mathcal{M}(A)$  (i.e., the differential lives in a section of the cotangent bundle over  $\mathcal{M}(A)$ ) defined as  $DC_B(X) : T_X \mathcal{M}(A) \rightarrow \mathbb{R}$  and the Riemannian metric  $\langle \cdot, \cdot \rangle$ , the inner product of the Riemannian gradient and any tangent vector  $\Omega \in T_X \mathcal{M}(A)$  in the tangent space is consistent with the directional derivative of  $C_B$  at  $X$  denoted as  $DC_B|_X(\Omega) = DC_B(X) \cdot \Omega$ ,

$$DC_B(X) \cdot \Omega = \langle \text{grad } C_B(X), \Omega \rangle, \forall \Omega \in T_X \mathcal{M}(A).$$

Intuitively, this condition states that the rate of change of the cost function  $C_B$  at the point  $X$  in the direction of any tangent vector  $\Omega \in T_X \mathcal{M}(A)$  (i.e., the directional derivative) is equal to how well the Riemannian gradient aligns with the given tangent vector  $\Omega$  in terms of the defined Riemannian metric.

See Fig. 2 for schematic views on the two conditions. In our setting, the tangent space of  $\mathcal{M}(A)$  at  $X \in \mathcal{M}(A)$  is given by

$$T_X \mathcal{M}(A) = \{[X, \xi] | \xi^\dagger = -\xi\}. \quad (\text{B4})$$

See Lemma 1.3 of Ref. [50] for the proof. Then, since the differential is given by  $DC_B|_X([X, \Omega]) = -\text{Tr}[[X, B]^\dagger \Omega]$ , the compatibility condition indicates that

$$-\text{Tr}[[X, B]^\dagger \Omega] = \langle \text{grad } C(X), \Omega \rangle = \langle [X, \xi], [X, \Omega] \rangle = \text{Tr}[\xi^\dagger \Omega], \quad (\text{B5})$$

where we use the normal Riemannian metric defined as  $\langle [X, \Omega_1], [X, \Omega_2] \rangle = \text{Tr}[\Omega_1^\dagger \Omega_2]$  for  $[X, \Omega_1], [X, \Omega_2] \in T_X \mathcal{M}(A)$ . As a result, Eq. (B5) reveals that  $\xi = [B, X]$ . Thus, we arrive at Eq. (B3): see Refs. [50, 71] for a detailed derivation. This suggests that the right-hand side of Eq. (B3) represents the steepest descent direction of the cost function on the Riemannian manifold  $\mathcal{M}(A)$ . The steepest descent flow is defined as the trajectory  $A(t) \in \mathcal{M}(A)$  satisfying

$$\frac{\partial A(t)}{\partial t} = \text{grad}_{A(t)} C_B(A(t)), \quad (\text{B6})$$

which leads to the differential equation

$$\frac{\partial A(t)}{\partial t} = [[A(t), B], A(t)] \quad (\text{B7})$$

known as the DBF.

Next, we show that ITE takes the form of a DBF. For clarity, we recall the definition of ITE. Given a target Hamiltonian  $\hat{H}$  and an initial state  $\Psi(0)$ , the ITE state can be written as

$$|\Psi(\tau)\rangle = \frac{e^{-\tau\hat{H}} |\Psi(0)\rangle}{\|e^{-\tau\hat{H}} |\Psi(0)\rangle\|} \quad (\text{B8})$$

for  $\tau \in \mathbb{R}$ . Then, by taking the derivative of Eq. (B8), we have

$$\begin{aligned} \frac{\partial |\Psi(\tau)\rangle}{\partial \tau} &= \frac{-\hat{H}e^{-\tau\hat{H}} |\Psi(0)\rangle}{\|e^{-\tau\hat{H}} |\Psi(0)\rangle\|} + \frac{e^{-\tau\hat{H}} |\Psi(0)\rangle \cdot \left( -\frac{\partial}{\partial \tau} \|e^{-\tau\hat{H}} |\Psi(0)\rangle\| \right)}{\|e^{-\tau\hat{H}} |\Psi(0)\rangle\|^2} \\ &= -\hat{H}|\Psi(\tau)\rangle + \frac{\langle \Psi(0) | \hat{H} e^{-2\tau\hat{H}} |\Psi(0)\rangle}{\|e^{-\tau\hat{H}} |\Psi(0)\rangle\|^2} |\Psi(\tau)\rangle \\ &= -\hat{H}|\Psi(\tau)\rangle + \langle \Psi(\tau) | \hat{H} |\Psi(\tau)\rangle |\Psi(\tau)\rangle \\ &= -(\hat{H} - E(\tau)I) |\Psi(\tau)\rangle \\ &= -[\hat{H}, \Psi(\tau)] |\Psi(\tau)\rangle \end{aligned} \quad (\text{B9})$$

with  $E(\tau) = \langle \Psi(\tau) | \hat{H} |\Psi(\tau)\rangle$  and  $\|e^{-\tau\hat{H}} |\Psi(0)\rangle\| = \sqrt{\langle \Psi(0) | e^{-2\tau\hat{H}} |\Psi(0)\rangle}$ . Finally, the density matrix representation of Eq. (B9) using  $\Psi(\tau) = |\Psi(\tau)\rangle \langle \Psi(\tau)|$  reveals that

$$\frac{\partial \Psi(\tau)}{\partial \tau} = [[\Psi(\tau), \hat{H}], \Psi(\tau)], \quad (\text{B10})$$

which is the exact form of DBF, as shown in Eq. (B7). Namely, ITE can be interpreted as the DBF with  $A = \Psi(\tau)$  and  $B = \hat{H}$  after setting  $\Psi(0) = |\psi_0\rangle\langle\psi_0|$ . Since DBF represents the steepest descent direction of the cost in Eq. (B2), ITE corresponds to the Riemannian gradient flow of the same least-squares cost. We can verify this by rewriting the cost function as

$$\begin{aligned} C_{\hat{H}}(\Psi(\tau)) &= -\frac{1}{2}\|\Psi(\tau) - \hat{H}\|_{\text{HS}}^2 \\ &= \underbrace{-\frac{1}{2}\|\Psi(\tau)\|_{\text{HS}}^2 - \frac{1}{2}\|\hat{H}\|_{\text{HS}}^2}_{\text{const.}} + \underbrace{\text{Tr}[\Psi(\tau)\hat{H}]}_{=E(\tau)}. \end{aligned} \quad (\text{B11})$$

Thus, Eq. (B11) shows that minimizing the least-squares cost is equivalent to minimizing the energy expectation value  $E(\tau)$ , which aligns with the objective of ITE, that is, ground-state preparation.

Lastly, we elaborate on the case for the unstructured search task. As shown in Lemma 1, the ITE state for unstructured search is given by

$$|\Phi(\tau)\rangle = \frac{e^{\tau\hat{H}_f}}{\sqrt{\langle\psi_0|e^{2\tau\hat{H}_f}|\psi_0\rangle}} |\psi_0\rangle, \quad (\text{B12})$$

where  $\hat{H}_f = \sum_{x \in \{x|f(x)=1\}} |x\rangle\langle x|$ . In this case, using  $\Phi(\tau) = |\Phi(\tau)\rangle\langle\Phi(\tau)|$  and  $\Phi(0) = |\psi_0\rangle\langle\psi_0|$ , its continuous differential equation form is expressed as

$$\frac{\partial\Phi(\tau)}{\partial\tau} = \left[ [\hat{H}_f, \Phi(\tau)], \Phi(\tau) \right], \quad (\text{B13})$$

which corresponds to the minimization of the cost

$$C_{\hat{H}_f}(\Psi) = \frac{1}{2}\|\hat{H}_f - \Psi\|_{\text{HS}}^2. \quad (\text{B14})$$

This is consistent with the goal of unstructured search that aims to identify the items satisfying  $f(x) = 1$ ; that is, to find the eigenvectors corresponding to the largest eigenvalues.

We note a subtle sign difference between the cost functions in Eq. (B11) and Eq. (B14). This discrepancy reflects the fact that ITE typically targets the ground state (the eigenstate with the smallest eigenvalue), whereas unstructured search seeks the largest-eigenvalue states. Nevertheless, both objectives can be expressed within the same formalism. By rewriting the cost function as

$$\tilde{C}_{\hat{H}_f}(\Psi) = -\frac{1}{2}\|(-\hat{H}_f) - \Psi\|_{\text{HS}}^2, \quad (\text{B15})$$

we effectively transform the task of maximization into a minimization problem similar to the ITE formulation for the ground-state preparation with  $\hat{H} = -\hat{H}_f$ .

## 2. Review of product formula for commutators

We here give an overview of known product formulae for exponentials of commutators, following Refs. [56–58].

First, we provide the second-order formula known as group commutator formula:

$$e^{sA}e^{sB}e^{-sA}e^{-sB} = e^{s^2[A,B]} + \mathcal{O}(s^3). \quad (\text{B16})$$

Using the identity  $[iB, iA] = [A, B]$ , we can also obtain the following approximation;

$$e^{isB}e^{isA}e^{-isB}e^{-isA} = e^{s^2[A,B]} + \mathcal{O}(s^3). \quad (\text{B17})$$

Next, we recall the third-order formula for the pure commutator:

$$e^{\phi sA}e^{\phi sB}e^{-sA}e^{-(\phi+1)sB}e^{(1-\phi)sA}e^{sB} = e^{s^2[A,B]} + \mathcal{O}(s^4) \quad (\text{B18})$$

with  $\phi = (\sqrt{5} - 1)/2$ .

Moreover, we can improve the order in recursive manners. Given a  $n$ -th order formula  $f_n(x) = \exp(s^2[A, B] + \mathcal{O}(s^{n+1}))$ , the following recursive formulae are known:

- 2 copies formula (for even  $n = 2k$ )

$$\begin{aligned} f_{n+1}(s) &= \exp(s^2[A, B] + \mathcal{O}(s^{n+2})) \\ &= f_n(s/\sqrt{2})f_n(-s/\sqrt{2}) \end{aligned} \quad (\text{B19})$$

- The Jean-Koseleff formula

$$\begin{aligned} f_{n+1}(s) &= \exp(s^2[A, B] + \mathcal{O}(s^{n+2})) \\ &= f_n(ts)f_n(ws)f_n(ts) \text{ (if } n \text{ is even)} \\ &= f_n(us)f_n(vs)^{-1}f_n(us) \text{ (if } n \text{ is odd)} \end{aligned} \quad (\text{B20})$$

with  $t = (2 + 2^{2/(n+1)})^{-1/2}$ ,  $w = -2^{1/(n+1)}t$ ,  $u = (2 - 2^{2/(n+1)})^{-1/2}$  and  $v = 2^{1/(n+1)}u$ .

- 5-copies formula

$$\begin{aligned} f_{n+1}(s) &= \exp(s^2[A, B] + \mathcal{O}(s^{n+2})) \\ &= f_n(\nu s)^2 f_n(\mu s)^{-1} f_n(\nu s)^2 \end{aligned} \quad (\text{B21})$$

with  $\mu = (4\sigma)^{1/2}$ ,  $\nu = (1/4 + \sigma)^{1/2}$  and  $\sigma = 4^{2/(n+1)}/(4(4 - 4^{2/(n+1)}))$ .

See Ref. [72] for an example of how alternative product formulae, originally developed in the context of pure mathematics [73, 74], have been applied. As a related aside, Ref. [75] provides an example of randomized compilation techniques employed in a similar context. By combining the techniques mentioned above, we can construct higher-order approximations of exponentials of commutators. These approximations generally take the form

$$e^{it_1 A} e^{it_2 B} e^{it_3 A} e^{it_4 B} \dots = e^{s^2[A, B]} + \mathcal{O}(s^m) \quad (\text{B22})$$

with appropriately chosen coefficients  $\{t_i\}$  to achieve an approximation of order  $m$ .

Lastly, we give an example to demonstrate the link between the approximation of ITE of Eq. (7) and the existing algorithms, especially the original Grover's algorithm. As a simple approach, we utilize the group commutator formula in Eq. (B16) together with the fragmentation for the approximation;

$$e^{s[\hat{H}_f, |\psi_0\rangle\langle\psi_0|]} \approx \left( e^{i\sqrt{2s/\mathcal{N}}|\psi_0\rangle\langle\psi_0|} e^{i\sqrt{2s/\mathcal{N}}\hat{H}_f} e^{-i\sqrt{2s/\mathcal{N}}|\psi_0\rangle\langle\psi_0|} e^{-i\sqrt{2s/\mathcal{N}}\hat{H}_f} \right)^{\mathcal{N}/2}. \quad (\text{B23})$$

In the original Grover's algorithm [1], the phase angles are  $\alpha_k = \beta_k = \pi$  for all  $k$ . Observing that

$$e^{i\pi\hat{H}_f} = I + (e^{i\pi} - 1)\hat{H}_f = I + (e^{-i\pi} - 1)\hat{H}_f = e^{-i\pi\hat{H}_f},$$

$$e^{i\pi|\psi_0\rangle\langle\psi_0|} = I + (e^{i\pi} - 1)|\psi_0\rangle\langle\psi_0| = I + (e^{-i\pi} - 1)|\psi_0\rangle\langle\psi_0| = e^{-i\pi|\psi_0\rangle\langle\psi_0|},$$

we can choose  $\sqrt{2s/\mathcal{N}} = \pi$  to match the structure of the original algorithm. This observation implies that Grover's algorithm can be interpreted as an approximation to the unitary generated by the commutator, i.e.,  $e^{s[\hat{H}_f, |\psi_0\rangle\langle\psi_0|]}$  with  $s = \pi^2\mathcal{N}/2$ .

Given these large angles, one might expect that the product formula approximation might not work. Nevertheless, the approximation technique works for some cases of unstructured search. Ref. [33] provides a general bound for the exponential of commutators;

$$\left\| e^{i\sqrt{s}\Psi} e^{i\sqrt{s}\hat{H}} e^{-i\sqrt{s}\Psi} e^{-i\sqrt{s}\hat{H}} - e^{s[\hat{H}, \Psi]} \right\|_{\text{op}} \leq s^{3/2} \left( \left\| [\hat{H}, [\hat{H}, \Psi]] \right\|_{\text{op}} + \left\| [\Psi, [\Psi, \hat{H}]] \right\|_{\text{op}} \right) \quad (\text{B24})$$

where  $s \geq 0$ ,  $\Psi$  is the density matrix and  $\hat{H}$  denotes an arbitrary Hermitian matrix. Here,  $\|\cdot\|_{\text{op}}$  represents the operator norm. Applying this to our case,  $s = \pi^2$ ,  $\Psi = |\psi_0\rangle\langle\psi_0|$  and  $\hat{H} = \hat{H}_f$  given  $\mathcal{N} = 2$ , we obtain the bound

$$\|e^{i\pi\psi_0} e^{i\pi\hat{H}_f} e^{-i\pi\psi_0} e^{-i\pi\hat{H}_f} - e^{\pi^2[\hat{H}_f, \psi_0]}\| \leq 2\pi^3 \|[\hat{H}_f, \psi_0]\| \quad (\text{B25})$$

$$\leq 4\pi^3 \sqrt{V_0}, \quad (\text{B26})$$

where  $V_0 = \langle\psi_0|(\hat{H}_f - E_0)^2|\psi_0\rangle = E_0(1 - E_0)$  and  $E_0 = M/N$ . For further details of the calculation, see App. C4. This demonstrates that the variance  $V_0$  fully governs the error of the product formula. Thus, when the number of target items  $M$  is small compared to the total number  $N$  (i.e.,  $V_0 = \Theta(1/N)$ ), which is the case of primary interest, the error remains small and the product formula can be highly accurate. On the other hand, when  $M$  is comparable to  $N$ , i.e.,  $V_0 \in \Theta(1)$ , the error grows accordingly and hence the approximation fails. This behavior suggests a potential for overshooting: as the state approaches the solution, the error introduced by the approximation increases, potentially preventing convergence to the solution state.

### 3. Overview on Geometry of Manifolds

In this section, we give an overview of the relationships among the manifolds discussed in the main text: the set of matrices  $\mathcal{M}(A)$  in Eq. (B1) generated by unitary evolution of a Hermitian operator  $A$ , the special unitary group  $SU(N)$ , the complex projective spaces  $\mathbb{C}\mathbb{P}$  and  $\mathbb{C}\mathbb{P}^{N-1}$ . Our discussion presented below follows Refs. [50, 59, 76].

**Link between the set  $\mathcal{M}(A)$  and the special unitary group  $SU(N)$**  – We first clarify the relationship between the set  $\mathcal{M}(A)$  and the special unitary group  $SU(N)$ . Here, we follow the discussion on Ref. [50]. Let us recall their definitions:

$$U(N) = \{U \in \mathbb{C}^{N \times N} | UU^\dagger = I\},$$

$$\mathcal{M}(A) = \{UAU^\dagger | U \in U(N)\},$$

$$SU(N) = \{U \in U(N) | \det(U) = 1\}.$$

Since  $e^{i\theta} UAU^\dagger e^{-i\theta} = UAU^\dagger$ , we have the equality  $\{UAU^\dagger | U \in U(N)\} = \{UAU^\dagger | U \in SU(N)\}$ . Then,  $\mathcal{M}(A)$  is an *orbit* space of the group action of  $SU(N)$  on  $\mathbb{C}^{N \times N}$ . In differential geometry, the orbit space of  $\sigma : G \times \mathcal{M} \rightarrow \mathcal{M}$  with a compact Lie group  $G$  and a smooth manifold  $\mathcal{M}$ , is generally defined as the set of all equivalence classes of  $\mathcal{M}$ ; namely  $\mathcal{M}/G \equiv \{O(x) | x \in \mathcal{M}\}$  with  $O(x) = \{g \cdot x | g \in G\}$  the orbit of  $x \in \mathcal{M}$ . Suppose the smooth Lie group action  $\sigma : SU(N) \times \mathbb{C}^{N \times N} \rightarrow \mathbb{C}^{N \times N}$  defined as  $\sigma_H(U) = UHU^\dagger$ ,  $H \in \mathcal{M}(A)$ . Then, we can easily see that  $\mathcal{M}(A)$  is an *orbit* of the group action  $\sigma$ . Roughly speaking,  $\mathcal{M}(A)$  describes the quotient of the space by the group action of  $SU(N)$ . We note that the link is used to show the set  $\mathcal{M}(A)$  is a smooth and compact manifold.  $\mathcal{M}(A)$  is a *homogeneous* space, meaning there exists a transitive group action: for any  $H_1, H_2 \in \mathcal{M}(A)$ , there exists  $U \in SU(N)$  such that  $H_2 = UH_1U^\dagger$ . It is well known that orbits of a compact Lie group acting on a manifold are themselves smooth, compact submanifolds. Since  $SU(N)$  is a compact Lie group,  $\mathcal{M}(A)$  is indeed a smooth and compact manifold.

We also recall that the stabilizer subgroup  $\text{Stab}(N) \subset SU(N)$  of  $A \in \mathbb{C}^{N \times N}$  is defined as

$$\text{Stab}(N) = \{U \in SU(N) | UAU^\dagger = A\}.$$

This subgroup consists of elements that leave  $A$  invariant under the action. With the subgroup, the orbit  $\mathcal{M}(A)$  is diffeomorphic to the homogeneous space, i.e.,

$$\mathcal{M}(A) \cong SU(N)/\text{Stab}(A).$$

Namely, there exists a continuous differentiable map  $f : \mathcal{M}(A) \rightarrow SU(N)/\text{Stab}(A)$  that is a bijection and its inverse is also differentiable.

Furthermore, we discuss the connection between these manifolds in terms of their tangent spaces. Since the map  $\sigma$  is a submersion (see e.g., App. C.6 of Ref. [50] for its definition), its differential at the identity induces a surjective linear map on tangent spaces. Note that the tangent space of  $SU(N)$  at the identity  $I$  is the Lie algebra:  $\mathfrak{su}(N) = T_I SU(N) = \{\Omega \in \mathbb{C}^{N \times N} | \Omega^\dagger = -\Omega, \text{Tr}[\Omega] = 0\}$ . Then, the derivative of  $\sigma_H(U) = UHU^\dagger$  at  $I$  is the surjective linear map  $D\sigma_H|_I : T_I SU(N) \rightarrow T_H \mathcal{M}(A)$  for  $H \in \mathcal{M}$  defined as

$$D\sigma_H|_I(\Omega) = \Omega H - H\Omega = [\Omega, H].$$

This suggests that elements in the tangent space of the set  $\mathcal{M}(A)$  at  $H \in \mathcal{M}(A)$  can be obtained from those in the tangent space of  $SU(N)$  at the identity. Using the expression together with the tangency and compatibility conditions, the Riemannian gradient flow in App. B1 is derived [50]. Similarly, Ref. [71] derives the Riemannian gradient flow on  $SU(d)$  in the context of the ground-state preparation. Their result coincides with the formulation given in Ref. [23], where the manifold  $\mathcal{M}(A)$  is explicitly considered for the same ground-state preparation task.

**Relation of set  $\mathcal{M}(A)$  and the special unitary group  $SU(N)$  to the complex projective space  $\mathbb{C}\mathbb{P}^{N-1}$**  – We now argue how the manifolds discussed above relate to the complex projective space. Let  $\mathbb{C}^N$  be the complex vector space of dimension  $N$ . The complex projective space  $\mathbb{C}\mathbb{P}^{N-1}$  is defined as the set of equivalence class of non-zero vectors in  $\mathbb{C}^N$ , where two vectors are considered equivalent if these vectors differ by a non-zero complex scalar factor. Formally,  $\mathbb{C}\mathbb{P}^{N-1} = (\mathbb{C}^N \setminus \{0\}) / \sim$ , where

$$y \sim x \iff y = \lambda x$$

for some  $\lambda \in \mathbb{C} \setminus \{0\}$ . The manifold naturally arises in the context of quantum mechanics, as pure quantum states are defined only up to a global phase. That is, the state vectors  $|\psi\rangle$  and  $e^{i\theta}|\psi\rangle$  are physically indistinguishable for  $\theta \in \mathbb{R}$ . Consequently, complex projective space plays a central role in analyzing the geometric structures in quantum mechanics [59].

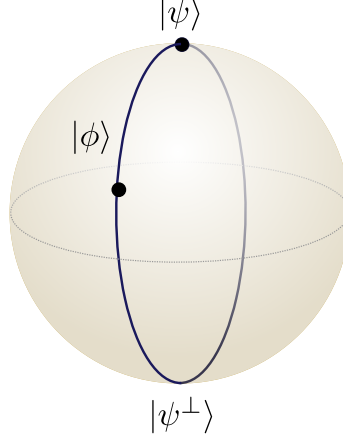


FIG. 3. **Schematic view of a geodesic on the Bloch sphere.** Given two pure states  $|\phi\rangle, |\psi\rangle \in \mathbb{C}^2$ , the geodesic in the complex projective space equipped with the Fubini-Study metric traces a great circle on the Bloch sphere. Here,  $|\psi^\perp\rangle$  denotes a state orthogonal to  $|\psi\rangle$ , i.e.,  $\langle\psi|\psi^\perp\rangle = 0$ . More generally, in  $\mathbb{C}P^{N-1}$ , the geodesic always lies within a two-dimensional subspace spanned by two quantum states.

The complex projective space admits the diffeomorphisms [76], i.e.,  $\mathbb{C}P^{N-1} \cong U(N)/(U(1) \times U(N-1)) \cong SU(N)/S(U(1) \times U(N-1))$ , with the subgroup  $S(U(1) \times U(N-1)) = \{(e^{i\theta}, V) \in U(1) \times U(N-1) | e^{i\theta} \det(V) = 1\}$ . This establishes a direct geometric link between complex projective space and quotient spaces of both the unitary and special unitary groups. Moreover, when the Hermitian operator  $A$  is the density matrix of a pure state (a rank-one Hermitian projector with unit trace) as is the case in ground-state preparation, the set  $\mathcal{M}(A)$  is diffeomorphic to  $\mathbb{C}P^{N-1}$  since  $\text{Stab}(A) = S(U(1) \times U(N-1))$ .

**Geodesics on  $\mathbb{C}P^{N-1}$  and its link to  $\mathbb{C}P^1$**  – Lastly, we mention the connection between  $\mathbb{C}P^{N-1}$  and  $\mathbb{C}P^1$  to ensure that Theorem 3 indeed shows that ITE follows a geodesic in  $\mathbb{C}P^{N-1}$ . Equipped with the Fubini-Study metric, the distance on the complex projective space for two states  $|\psi\rangle, |\phi\rangle$  in complex projective space  $\mathbb{C}P^{N-1}$  is given by

$$d_{\text{FS}}(|\psi\rangle, |\phi\rangle) = \arccos(|\langle\psi|\phi\rangle|). \quad (\text{B27})$$

In this case, it is known that the geodesic in  $\mathbb{C}P^{N-1}$  between two points lies within a submanifold isomorphic to  $\mathbb{C}P^1$  known as a complex projective line [59]. Intuitive understanding of this result is as follows. From Eq. (B27), we observe that the Fubini-Study distance between two pure states depends only on angle of their overlap; that is, any states lying outside two-dimensional complex subspace spanned by them do not affect the overlap and only increases the path length. Since a geodesic minimizes the distance locally, it must lie entirely within the span of the two states. Fig. 3 illustrates the geodesic in the case of a single-qubit system, i.e., the geodesic on the Bloch sphere (the complex projective space  $\mathbb{C}P^1$ ) as an example.

This  $\mathbb{C}P^1$  plays a role analogous to a “great circle” on a sphere, capturing the minimal-length path in the curved geometry of projective space. In our case, Eq. (13) represents the unitary evolution within a two-dimensional subspace of  $\mathbb{C}^N$ , which projects down to a  $\mathbb{C}P^1$  in  $\mathbb{C}P^{N-1}$ . Since the target state lies along this path, the evolution indeed follows a geodesic in the complex projective space.

#### 4. Overview of Quantum Signal Processing

Here, we elaborate on quantum signal processing (QSP) [30]. In the original work, a quantum circuit  $U_{QSP}$  was introduced with a sequential structure comprising of two types of operators: *signal operators*  $W$  and *signal processing operators*  $S(\phi)$ , where the phase  $\phi$  is drawn from a set  $\phi_k$ . The desired polynomial transformation is then obtained by performing a measurement in the so-called *signal basis*. Consider a degree- $K$  polynomial of a scalar input  $x \in [-1, 1]$ . Then, it was demonstrated that there exists a sequence of QSP phases  $\{\phi_k\}$  such that the following circuit

$$U_{QSP} = S_z(\phi_K) \prod_{k=0}^{K-1} W(x) S_z(\phi_k) \quad (\text{B28})$$

with the operators

$$W(x) = e^{ixX/2} = \begin{pmatrix} x & i\sqrt{1-x^2} \\ i\sqrt{1-x^2} & x \end{pmatrix},$$

$$S_z(\phi) = e^{i\phi Z} = \begin{pmatrix} e^{i\phi} & 0 \\ 0 & e^{-i\phi} \end{pmatrix}, \quad (\text{B29})$$

followed by measurement in the computational basis  $M = \{|0\rangle, |1\rangle\}$  can realize any polynomial  $p(x) \in \mathbb{C}[x]$  of degree- $K$ , provided that

1. Degree of  $p(x)$  is equal to or less than  $K$ ,
2.  $p(x)$  has a parity  $K \bmod 2$ ,
3.  $\forall x \in [-1, 1], |p(x)| \leq 1$ ,
4.  $\forall x \in (-\infty, -1] \cup [1, \infty), |p(x)| \geq 1$ ,
5. if  $K$  is even, then  $\forall x \in \mathbb{R}, |p(ix)p^*(ix)| \geq 1$ .

We refer to the setting as  $(R(x), S_Z, |0\rangle)$ -QSP. When the target polynomial is real, choosing the basis  $M = \{|+\rangle, |-\rangle\}$  allows the function to be implemented by considering the first three of the above five conditions only. The  $(R(x), S_Z, |+\rangle)$ -QSP convention is often preferred in practice, as it allows for a broader class of achievable functions compared to the  $(R(x), S_Z, |0\rangle)$ -QSP setting.

Equivalently, we can use the notation

$$R(x) = \begin{pmatrix} x & \sqrt{1-x^2} \\ \sqrt{1-x^2} & -x \end{pmatrix} \quad (\text{B30})$$

to have the equality

$$S_z(\phi_K) \prod_{k=0}^{K-1} W(x) S_z(\phi_k) = S_z(\phi'_K) \prod_{k=0}^{K-1} R(x) S_z(\phi'_k) \quad (\text{B31})$$

with the relationship  $R(x) = -ie^{i\pi Z/4}W(x)e^{i\pi Z/4}$  and hence  $\phi'_K = \phi_K + (2K-1)\pi/4$ ,  $\phi'_0 = \phi_0 - \pi/4$  and  $\phi'_k = \phi_k - \pi/2$  for  $k = 1, \dots, K-1$ . See Ref. [19, 28–31] for more details.

## Appendix C: Proofs in the Main Texts

### 1. Proof of Lemma 1

For completeness, we provide the statement from the main text again.

**Lemma C.1** (ITE solves the unstructured search problem). *Given the projector Hamiltonian  $\hat{H}_f$  in Eq. (A4) and the initial state in Eq. (A1), the ITE state*

$$|\psi(\tau)\rangle = \frac{e^{\tau\hat{H}_f} |\psi_0\rangle}{\|e^{\tau\hat{H}_f} |\psi_0\rangle\|_2} \quad (\text{C1})$$

with  $\|e^{\tau\hat{H}_f} |\psi_0\rangle\|_2 = \sqrt{\langle\psi_0|e^{2\tau\hat{H}_f}|\psi_0\rangle}$  converges to the solution state in Eq. (A5) as  $\tau \rightarrow \infty$ , i.e.,

$$\lim_{\tau \rightarrow \infty} \frac{e^{\tau\hat{H}_f} |\psi_0\rangle}{\|e^{\tau\hat{H}_f} |\psi_0\rangle\|_2} = |\psi^*\rangle. \quad (\text{C2})$$

*Proof.* By taking the limit  $\tau \rightarrow \infty$  of Eq. (C1), we have

$$\begin{aligned} \lim_{\tau \rightarrow \infty} \frac{e^{\tau\hat{H}_f}}{\sqrt{\langle\psi_0|e^{2\tau\hat{H}_f}|\psi_0\rangle}} |\psi_0\rangle &= \lim_{\tau \rightarrow \infty} \frac{I + (e^\tau - 1)\hat{H}_f}{\sqrt{\langle\psi_0|I + (e^{2\tau} - 1)\hat{H}_f|\psi_0\rangle}} |\psi_0\rangle \\ &= \lim_{\tau \rightarrow \infty} \frac{I/e^\tau + (1 - 1/e^\tau)\hat{H}_f}{\sqrt{\langle\psi_0|I/e^{2\tau} + (1 - 1/e^{2\tau})\hat{H}_f|\psi_0\rangle}} |\psi_0\rangle \\ &= \frac{\hat{H}_f |\psi_0\rangle}{\sqrt{\langle\psi_0|\hat{H}_f|\psi_0\rangle}} \\ &= \frac{1}{\sqrt{M}} \sum_{x \in \{x|f(x)=1\}} |x\rangle = |\psi^*\rangle, \end{aligned} \quad (\text{C3})$$

where we use the equality

$$e^{\tau \hat{H}_f} = I + (e^\tau - 1)\hat{H}_f. \quad (\text{C4})$$

in the first equality. This identity holds because  $\hat{H}_f$  is a projector, i.e.,  $\hat{H}_f^2 = \hat{H}_f$ .  $\square$

Note that the convergence to the solution state  $|\psi^*\rangle$  is guaranteed when the initial state includes all the answer states with a uniform probability; otherwise, some solutions excluded from the initial state can not be obtained at the final step; for example, if the initial state is  $|0\rangle$  given  $f(0) = 1$ , the resultant state is different from the solution state, i.e.,  $\lim_{\tau \rightarrow \infty} |\psi(\tau)\rangle = |0\rangle$ .

## 2. Proof of Lemma 2

For clarity, we restate the result from the main text.

**Lemma C.2** ([ITE can be realized by its first-order approximation]). *Let  $\hat{H}_f$  be the projector Hamiltonian in Eq. (A4). Then, for any ITE evolution time  $\tau$ , there exists a time duration  $s_\tau$  such that*

$$\frac{e^{\tau \hat{H}_f} |\psi_0\rangle}{\|e^{\tau \hat{H}_f} |\psi_0\rangle\|} = e^{s_\tau [\hat{H}_f, \psi_0]} |\psi_0\rangle \quad (\text{C5})$$

for any  $\tau$ .

*Proof.* Our proof fundamentally relies on Lemma B.3 in Ref. [55], which we restate below for completeness:

**Lemma C.3** (Lemma B.3 in Ref. [55]). *Let  $x, y \in \mathbb{R}$  and  $(x, y) \neq (0, 0)$ . Define the parameter*

$$s = -\frac{\text{sgn}(y)}{\sqrt{V_\Psi}} \arccos \left( \frac{x + yE_\Psi}{\|(xI + yH)|\Psi\rangle\|} \right), \quad (\text{C6})$$

with  $E_\Psi = \langle \Psi | \hat{H} | \Psi \rangle$  and  $V_\Psi = \langle \Psi | (\hat{H} - E_\Psi)^2 | \Psi \rangle = \langle \Psi | \hat{H}^2 | \Psi \rangle - E_\Psi^2$ , given a state vector  $|\Psi\rangle$  and an arbitrary Hermitian matrix  $\hat{H}$ . Then,

$$\frac{(xI + y\hat{H})|\Psi\rangle}{\|(xI + y\hat{H})|\Psi\rangle\|} = (a(s)I + b(s)H)|\Psi\rangle = e^{s[\langle \Psi | \langle \Psi |, \hat{H}]} |\Psi\rangle, \quad (\text{C7})$$

where  $a(s), b(s)$  are real-valued coefficients given by

$$a(s) = \frac{E_\Psi}{\sqrt{V_\Psi}} \sin(s\sqrt{V_\Psi}) + \cos(s\sqrt{V_\Psi}), \quad (\text{C8})$$

$$b(s) = -\frac{1}{\sqrt{V_\Psi}} \sin(s\sqrt{V_\Psi}). \quad (\text{C9})$$

Considering a specific case of Lemma C.3, we have

$$\frac{(I + c\hat{H})|\Psi\rangle}{\|(I + c\hat{H})|\Psi\rangle\|} = e^{s[\hat{H}, |\Psi\rangle\langle \Psi|]} |\Psi\rangle \quad (\text{C10})$$

when

$$s = \frac{1}{\sqrt{V_\Psi}} \arccos \left( \frac{1 + cE_\Psi}{\|(I + cH)|\Psi\rangle\|} \right) \quad (\text{C11})$$

for  $c > 0$ . In our case, we consider the projector  $\hat{H} = \hat{H}_f$  and the initial state  $|\Psi\rangle = |\psi_0\rangle$  defined in Eq. (A1). Using the equality shown in Eq. (C4), the ITE state in Eq. (C1) can be simplified to

$$\frac{e^{\tau \hat{H}_f} |\psi_0\rangle}{\|e^{\tau \hat{H}_f} |\psi_0\rangle\|} = \frac{(I + (e^\tau - 1)\hat{H}_f)|\psi_0\rangle}{\|(I + (e^\tau - 1)\hat{H}_f)|\psi_0\rangle\|} \equiv \frac{(I + c\hat{H})|\Psi\rangle}{\|(I + c\hat{H})|\Psi\rangle\|} \quad (\text{C12})$$

with  $c = e^\tau - 1$ , suggesting that the existence of the time duration  $s_\tau$  such that the ITE state for unstructured search can be realized by the exponential of commutators in Eq. (C10), since  $e^\tau - 1 > 0$  for any  $\tau > 0$ . More concretely, using the time duration

$$s_\tau = \frac{1}{\sqrt{E_0(1-E_0)}} \arccos \left( \frac{1 + (e^\tau - 1)E_0}{\sqrt{1 + (e^{2\tau} - 1)E_0}} \right) \quad (\text{C13})$$

with  $E_0 = \langle \psi_0 | \hat{H} | \psi_0 \rangle$  and  $V_0 = \langle \psi_0 | \hat{H}^2 | \psi_0 \rangle - E_0 = E_0(1 - E_0)$ , the equality in Eq. (C5) holds for any  $\tau$ .  $\square$

Additionally, we investigate how the imaginary time  $\tau$  relates to the corresponding time duration  $s_\tau$ , to gain insights into the trajectories of the ITE and its first-order approximation. By computing the derivative of Eq. (C13), we have

$$\begin{aligned} \frac{ds_\tau}{d\tau} &= \underbrace{\frac{1}{\sqrt{E_0(1-E_0)}}}_{a} \cdot \underbrace{\left( \frac{-1}{\sqrt{1 - \left( \frac{1+(e^\tau-1)E_0}{\sqrt{1+(e^{2\tau}-1)E_0}} \right)^2}} \right)}_{b} \cdot \underbrace{\frac{d}{d\tau} \left( \frac{1 + (e^\tau - 1)E_0}{\sqrt{1 + (e^{2\tau} - 1)E_0}} \right)}_{c}, \\ &= abc, \end{aligned} \quad (\text{C14})$$

where we use the equality  $d(\arccos(x))/dx = -1/\sqrt{1-x^2}$ . Since  $E_0$  ranges from 0 to 1,  $ab$  is always negative for  $\tau > 0$ . As for the term  $c$ , we can obtain

$$\begin{aligned} \frac{d}{d\tau} \left( \frac{1 + (e^\tau - 1)E_0}{\sqrt{1 + (e^{2\tau} - 1)E_0}} \right) &= \frac{e^\tau E_0 \left( \sqrt{1 + (e^{2\tau} - 1)E_0} \right) - (1 + (e^\tau - 1)E_0) \frac{e^{2\tau} E_0}{\sqrt{1 + (e^{2\tau} - 1)E_0}}}{1 + (e^{2\tau} - 1)E_0} \\ &= \frac{E_0 e^\tau (1 + (e^{2\tau} - 1)E_0) - E_0 e^{2\tau} (1 + (e^\tau - 1)E_0)}{(1 + (e^{2\tau} - 1)E_0)^{3/2}} \\ &= \frac{-E_0 e^\tau (1 - E_0)(e^\tau - 1)}{(1 + (e^{2\tau} - 1)E_0)^{3/2}} \leq 0. \end{aligned} \quad (\text{C15})$$

Consequently, combining the above results, the derivative of the time duration is non-negative, i.e.,  $ds_\tau/d\tau \geq 0$  for all  $\tau \geq 0$ . Note that  $s_\tau = 0$  when  $\tau = 0$ . Thus,  $s_\tau$  is increasing from 0 and reaches a plateau for a large value of  $\tau$  (as  $\lim_{\tau \rightarrow \infty} ds_\tau/d\tau = 0$ ). This suggests that the time duration  $s_\tau$  increases with  $\tau$ , but eventually saturates, reflecting a deviation between the ITE and its first-order approximation; the latter overshoots the ITE trajectory.

### 3. Proof of Theorem 3

To aid readability, we restate the formulation introduced earlier.

**Theorem C.4** (ITE traces the geodesic). *Let  $\hat{H}_f$  be the projector in Eq. (A4) and  $|\psi_0\rangle$  be the initial state defined in Eq. (A1). Define the orthonormal state*

$$|\psi_0^\perp\rangle = \frac{\hat{H}_f - E_0 I}{\sqrt{E_0(1-E_0)}} |\psi_0\rangle \quad (\text{C16})$$

such that  $\langle \psi_0 | \psi_0^\perp \rangle = 0$ , where  $E_0 = \langle \psi_0 | \hat{H}_f | \psi_0 \rangle = M/N$ . Then, the ITE state in Eq. (7) for a time duration  $s$  is given by

$$|\psi_s\rangle = \cos(s\sqrt{V_0}) |\psi_0\rangle + \sin(s\sqrt{V_0}) |\psi_0^\perp\rangle, \quad (\text{C17})$$

where  $V_0 = \langle \psi_0 | (\hat{H}_f - E_0)^2 | \psi_0 \rangle = E_0(1 - E_0)$ . Since Eq. (13) can realize the solution state  $|\psi^*\rangle$  when

$$s^* = \arccos(\sqrt{E_0})/\sqrt{V_0}, \quad (\text{C18})$$

ITE follows the trajectory of the geodesic on  $\mathbb{CP}^{N-1}$ .

*Proof.* We first show that the ITE dynamics can be expressed as Eq. (C17). We here utilize the proof shown in Lemma 1 of Ref. [55]. The exponential of the commutator  $\hat{W}_{\hat{H}} \equiv [\hat{H}, |\Psi\rangle\langle\Psi|]$  for an arbitrary Hermitian matrix  $\hat{H}$  and a state vector  $|\Psi\rangle$  can be expressed as

$$e^{s\hat{W}_{\hat{H}}} = \sum_{k=0}^{\infty} \frac{s^k}{k!} \hat{W}_{\hat{H}}^k. \quad (\text{C19})$$

Since

$$\hat{W}_{\hat{H}} |\Psi\rangle = \hat{H} |\Psi\rangle - E_{\Psi} |\Psi\rangle$$

and

$$\hat{W}_{\hat{H}}^2 |\Psi\rangle = \hat{W}_{\hat{H}} \hat{H} |\Psi\rangle - E_{\Psi} \hat{W}_{\hat{H}} |\Psi\rangle = E_{\Psi} \hat{H} |\Psi\rangle - \langle\Psi|\hat{H}^2|\Psi\rangle |\Psi\rangle - E_{\Psi} \hat{H} |\Psi\rangle + E_{\Psi}^2 |\Psi\rangle = -V_{\Psi} |\Psi\rangle$$

with  $E_{\Psi} = \langle\Psi|\hat{H}|\Psi\rangle$  and  $V_{\Psi} = \langle\Psi|(\hat{H} - E_{\Psi})^2|\Psi\rangle = \langle\Psi|\hat{H}^2|\Psi\rangle - E_{\Psi}^2$ , any even power of the commutator  $\hat{W}_{\hat{H}}$  acting on the state  $|\Psi\rangle$  gives

$$\hat{W}_{\hat{H}}^{2k} |\Psi\rangle = (-V_{\Psi})^k |\Psi\rangle. \quad (\text{C20})$$

Similarly, we have  $\hat{W}_{\hat{H}}^{2k+1} |\Psi\rangle = (-V_{\Psi})^k \hat{W}_{\hat{H}} |\Psi\rangle$  for any odd power. Therefore, separating the odd and even terms leads to a weighted sum of  $|\Psi\rangle$  and  $\hat{W}_{\hat{H}} |\Psi\rangle$  with coefficients expressed by sine and cosine functions as

$$e^{s\hat{W}_{\hat{H}}} |\Psi\rangle = \cos(s\sqrt{V_{\Psi}}) |\Psi\rangle + \sin(s\sqrt{V_{\Psi}}) \frac{\hat{W}_{\hat{H}}}{\sqrt{V_{\Psi}}} |\Psi\rangle. \quad (\text{C21})$$

In our case, we consider  $\hat{H} = \hat{H}_f$  and  $|\Psi\rangle = |\psi_0\rangle$  with  $E_0 = \langle\psi_0|\hat{H}_f|\psi_0\rangle$  and  $V_0 = \langle\psi_0|(\hat{H}_f - E_0)^2|\psi_0\rangle = E_0(1 - E_0)$ . Thus Eq. (C21) is re-expressed as

$$\begin{aligned} e^{s[\hat{H}_f, \psi_0]} |\psi_0\rangle &= \cos(s\sqrt{V_0}) |\psi_0\rangle + \sin(s\sqrt{V_0}) \frac{[\hat{H}_f, |\psi_0\rangle\langle\psi_0|]}{\sqrt{V_0}} |\psi_0\rangle \\ &= \cos(s\sqrt{V_0}) |\psi_0\rangle + \sin(s\sqrt{V_0}) |\psi_0^\perp\rangle. \end{aligned} \quad (\text{C22})$$

Next, we verify that there exists a time duration  $s$  such that the ITE state  $|\psi_s\rangle$  results in the solution state of Eq. (A5). By expressing Eq. (C22) solely in terms of  $|\psi_0\rangle$  and substituting  $V_0 = E_0(1 - E_0)$ , we have

$$|\psi_s\rangle = \left( \left( -\frac{E_0}{\sqrt{E_0(1 - E_0)}} \sin(s\sqrt{V_0}) + \cos(s\sqrt{V_0}) \right) I + \sin(s\sqrt{V_0}) \frac{\hat{H}_f}{\sqrt{E_0(1 - E_0)}} \right) |\psi_0\rangle. \quad (\text{C23})$$

Note that the solution state can be written as  $|\psi^*\rangle = \hat{H}_f |\psi_0\rangle / \sqrt{E_0}$ . Thus, by solving

$$-\frac{E_0}{\sqrt{E_0(1 - E_0)}} \sin(s\sqrt{V_0}) + \cos(s\sqrt{V_0}) = 0, \quad (\text{C24})$$

$$\frac{\sin(s\sqrt{V_0})}{\sqrt{E_0(1 - E_0)}} = \frac{1}{\sqrt{E_0}}, \quad (\text{C25})$$

i.e., computing (C24) + (C25)  $\times E_0$ , we obtain  $s^* = \arccos(\sqrt{E_0})/\sqrt{V_0}$ . These results suggest that ITE dynamics in Eq. (7) describes a great circle connecting the initial and the solution states.  $\square$

#### 4. Proof of Theorem 4

We restate the main result here to facilitate the discussion that follows.

**Theorem C.5** (Geodesic length of ITE determines query complexity of Grover's algorithm). *Given a projector Hamiltonian  $\hat{H}_f$ , consider the ITE evolution generated by the operator  $e^{s^*[\hat{H}_f, \psi_0]}$ , where the optimal time  $s^*$  of Eq. (C18) ensures that ITE reaches the solution state  $|\psi_{s^*}\rangle = |\psi^*\rangle$ . Then, there exists a Grover iteration  $\prod_{k=1}^{\mathcal{N}} G_k(\alpha_k, \beta_k)$  satisfying*

$$\left\| e^{s^*[\hat{H}_f, \psi_0]} - (-1)^{\mathcal{N}} \prod_{k=1}^{\mathcal{N}} G_k(\alpha_k, \beta_k) \right\|_{\text{op}} \leq \epsilon, \quad (\text{C26})$$

for the operator norm  $\|\cdot\|_{\text{op}}$  and any  $\epsilon \in (0, 2)$ , using the number of queries

$$\mathcal{N} \in \mathcal{O} \left( \frac{1}{\epsilon^2 |\pi/2 - d_{\text{FS}}|} \right) \quad (\text{C27})$$

where  $d_{\text{FS}} \equiv d_{\text{FS}}(|\psi_0\rangle, |\psi^*\rangle)$  is the geodesic length between the initial and solution states.

*Proof.* Consider the Grover iterations  $\prod_{k=1}^{\mathcal{N}} G_k(\alpha_k, \beta_k)$  with angles  $\alpha_{2k} = \beta_{2k} = -\alpha_{2k-1} = -\beta_{2k-1} = \sqrt{2s^*/\mathcal{N}}$ . Note that this set of angles are given by the simple approximation of the exponential of commutators using the group commutator and fragmentation; see App. B 2 for the detail. Without loss of generality, we also assume  $\mathcal{N}$  is even; for odd  $\mathcal{N}$ , setting the last angles as  $\alpha_{\mathcal{N}} = \beta_{\mathcal{N}} = 0$  reduces to the situation of the even case with one additional (i.e., constant) query. Then, the error bound of Eq. (C26) is rewritten as

$$\left\| e^{s^*[\hat{H}_f, |\psi_0\rangle\langle\psi_0|]} - \left( e^{i\sqrt{2s^*/\mathcal{N}}|\psi_0\rangle\langle\psi_0|} e^{i\sqrt{2s^*/\mathcal{N}}\hat{H}_f} e^{-i\sqrt{2s^*/\mathcal{N}}|\psi_0\rangle\langle\psi_0|} e^{-i\sqrt{2s^*/\mathcal{N}}\hat{H}_f} \right)^{\mathcal{N}/2} \right\|_{\text{op}} \leq \epsilon, \quad (\text{C28})$$

where  $\|\cdot\|_{\text{op}}$  represents the operator norm. The upper bound of Eq. (C28) is given by

$$\begin{aligned} & \left\| e^{s^*[\hat{H}_f, |\psi_0\rangle\langle\psi_0|]} - \left( e^{i\sqrt{2s^*/\mathcal{N}}|\psi_0\rangle\langle\psi_0|} e^{i\sqrt{2s^*/\mathcal{N}}\hat{H}_f} e^{-i\sqrt{2s^*/\mathcal{N}}|\psi_0\rangle\langle\psi_0|} e^{-i\sqrt{2s^*/\mathcal{N}}\hat{H}_f} \right)^{\mathcal{N}/2} \right\|_{\text{op}} \\ & \leq \frac{\mathcal{N}}{2} \left\| e^{\frac{2s^*}{\mathcal{N}}[\hat{H}_f, |\psi_0\rangle\langle\psi_0|]} - e^{i\sqrt{2s^*/\mathcal{N}}|\psi_0\rangle\langle\psi_0|} e^{i\sqrt{2s^*/\mathcal{N}}\hat{H}_f} e^{-i\sqrt{2s^*/\mathcal{N}}|\psi_0\rangle\langle\psi_0|} e^{-i\sqrt{2s^*/\mathcal{N}}\hat{H}_f} \right\|_{\text{op}} \\ & \leq \frac{\mathcal{N}}{2} \left( \frac{2s^*}{\mathcal{N}} \right)^{\frac{3}{2}} \left( \left\| [\hat{H}_f, [\hat{H}_f, |\psi_0\rangle\langle\psi_0|]] \right\|_{\text{op}} + \left\| [[\psi_0\rangle\langle\psi_0|, [\psi_0\rangle\langle\psi_0|], \hat{H}_f]] \right\|_{\text{op}} \right). \end{aligned} \quad (\text{C29})$$

In the first equality, we apply the telescoping followed by the triangle inequality  $\mathcal{N}/2$  times utilizing the fact that  $e^{\frac{2s^*}{\mathcal{N}}[\hat{H}_f, |\psi_0\rangle\langle\psi_0|]}$  and  $e^{i\sqrt{2s^*/\mathcal{N}}|\psi_0\rangle\langle\psi_0|} e^{i\sqrt{2s^*/\mathcal{N}}\hat{H}_f} e^{-i\sqrt{2s^*/\mathcal{N}}|\psi_0\rangle\langle\psi_0|} e^{-i\sqrt{2s^*/\mathcal{N}}\hat{H}_f}$  are unitary. Lastly, we use the inequality proved in Ref. [33];

$$\left\| e^{i\sqrt{s}\Psi} e^{i\sqrt{s}\hat{H}} e^{-i\sqrt{s}\Psi} e^{-i\sqrt{s}\hat{H}} - e^{s[\hat{H}, \Psi]} \right\|_{\text{op}} \leq s^{3/2} \left( \left\| [\hat{H}, [\hat{H}, \Psi]] \right\|_{\text{op}} + \left\| [\Psi, [\Psi, \hat{H}]] \right\|_{\text{op}} \right) \quad (\text{C30})$$

for the density matrix representation of a pure state  $\Psi = |\Psi\rangle\langle\Psi|$ , an arbitrary Hermitian matrix  $\hat{H}$  and  $s \geq 0$ . Note that

$$\begin{aligned} [\hat{H}_f, [\hat{H}_f, |\psi_0\rangle\langle\psi_0|]] &= [\hat{H}_f, \hat{H}_f |\psi_0\rangle\langle\psi_0| - |\psi_0\rangle\langle\psi_0| \hat{H}_f] \\ &= \hat{H}_f |\psi_0\rangle\langle\psi_0| - 2\hat{H}_f |\psi_0\rangle\langle\psi_0| \hat{H}_f + |\psi_0\rangle\langle\psi_0| \hat{H}_f, \end{aligned} \quad (\text{C31})$$

as  $\hat{H}_f$  is a projector, i.e.,  $\hat{H}_f^2 = \hat{H}_f$ . Since the Hilbert-Schmidt norm  $\|\cdot\|_{\text{HS}}$  always upper bounds the operator norm, we obtain

$$\begin{aligned} \left\| [\hat{H}_f, [\hat{H}_f, |\psi_0\rangle\langle\psi_0|]] \right\|_{\text{op}} &\leq \left\| [\hat{H}_f, [\hat{H}_f, |\psi_0\rangle\langle\psi_0|]] \right\|_{\text{HS}} \\ &\leq \left\| \hat{H}_f |\psi_0\rangle\langle\psi_0| - 2\hat{H}_f |\psi_0\rangle\langle\psi_0| \hat{H}_f + |\psi_0\rangle\langle\psi_0| \hat{H}_f \right\|_{\text{HS}} = \sqrt{2V_0}. \end{aligned} \quad (\text{C32})$$

Similarly, as

$$\begin{aligned} [[\psi_0\rangle\langle\psi_0|, [[\psi_0\rangle\langle\psi_0|, \hat{H}_f]]]] &= [[\psi_0\rangle\langle\psi_0|, |\psi_0\rangle\langle\psi_0| \hat{H}_f - \hat{H}_f |\psi_0\rangle\langle\psi_0|]] \\ &= \hat{H}_f |\psi_0\rangle\langle\psi_0| - 2E_0 |\psi_0\rangle\langle\psi_0| + |\psi_0\rangle\langle\psi_0| \hat{H}_f, \end{aligned} \quad (\text{C33})$$

we also have  $\left\| [\left| \psi_0 \right\rangle \langle \psi_0 |, [\left| \psi_0 \right\rangle \langle \psi_0 |, \hat{H}_f]] \right\|_{\text{op}} \leq \sqrt{2V_0}$ . Consequently, Eq. (C29) can be further bounded as follows;

$$\begin{aligned} \frac{\mathcal{N}}{2} \left( \frac{2s^*}{\mathcal{N}} \right)^{\frac{3}{2}} \left( \left\| [\hat{H}_f, [\hat{H}_f, \left| \psi_0 \right\rangle \langle \psi_0 |]] \right\|_{\text{op}} + \left\| [\left| \psi_0 \right\rangle \langle \psi_0 |, [\left| \psi_0 \right\rangle \langle \psi_0 |, \hat{H}_f]] \right\|_{\text{op}} \right) &\leq \frac{\mathcal{N}}{2} \left( \frac{2s^*}{\mathcal{N}} \right)^{\frac{3}{2}} \cdot 2\sqrt{2}\sqrt{V_0} \\ &= 4 \frac{\sqrt{V_0} s^{*3/2}}{\mathcal{N}^{1/2}} \\ &\leq 2\pi \left( \frac{s^*}{\mathcal{N}} \right)^{1/2}. \end{aligned} \quad (\text{C34})$$

In the last inequality, we use the relation  $s^* = \arccos(\sqrt{E_0})/\sqrt{V_0}$ , which implies  $\sqrt{V_0}s^* = \arccos(\sqrt{E_0}) \leq \pi/2$  since  $0 \leq \sqrt{E_0} \leq 1$ .

Now, we relate the upper bound to the geodesic length on the complex projective manifold with respect to the Fubini-Study metric;

$$d_{\text{FS}} = \arccos(|\langle \psi_0 | \psi^* \rangle|) = \arccos(\sqrt{E_0}). \quad (\text{C35})$$

Indeed, using the geodesic length in Eq. (C35), the optimal time duration can be expressed as

$$s^* = \arccos(\sqrt{E_0})/\sqrt{V_0} = \frac{d_{\text{FS}}}{\cos(d_{\text{FS}}) \sin(d_{\text{FS}})} = \frac{1}{\text{sinc}(2d_{\text{FS}})}, \quad (\text{C36})$$

with  $\text{sinc}(x) = \sin(x)/x$ . Here, from the definition of  $d_{\text{FS}}$  in Eq. (C35), we utilize the identities  $\cos(d_{\text{FS}}) = \sqrt{E_0}$  and  $\sin(d_{\text{FS}}) = \sqrt{1 - E_0}$  to rewrite  $V_0 = E_0(1 - E_0)$ . Then we have

$$\frac{1}{\text{sinc}(2x)} \leq \frac{2}{|\pi/2 - x|} \quad (\text{C37})$$

for  $0 \leq x \leq \pi/2$ . Thus, the upper bound of Eq. (C34) is further given by

$$2\pi \left( \frac{s^*}{\mathcal{N}} \right)^{1/2} \leq 2\sqrt{2}\pi \left( \frac{1}{\mathcal{N}|\pi/2 - d_{\text{FS}}|} \right)^{1/2}. \quad (\text{C38})$$

As a result, to achieve the error  $\epsilon$ , it suffices to have

$$\mathcal{N} = \left\lceil \frac{(2\sqrt{2}\pi)^2}{\epsilon^2} \frac{1}{|\pi/2 - d_{\text{FS}}|} \right\rceil. \quad (\text{C39})$$

□

Note that, in this case, the geodesic length on complex projective space coincides with that on the special unitary group with the bi-invariant metric up to a multiplicative constant. The geodesic between two unitary operators  $U, V$  on the special unitary group [77] is given by  $e^{i\Gamma t}$  for  $t \in [0, 1]$  with

$$\Gamma = -i \log(U^\dagger V). \quad (\text{C40})$$

Accordingly, the geodesic length is expressed as  $\|\log(U^\dagger V)\|_{\text{HS}}$ . In the context of unstructured search, we are interested in two unitary operators  $I$  and  $e^{s^*[\hat{H}_f, \left| \psi_0 \right\rangle \langle \psi_0 |]}$  with  $s^*$  of Eq. (C18), since actions of these operators on  $\left| \psi_0 \right\rangle$  yield the initial and the solution states, respectively i.e.,  $\left| \psi_0 \right\rangle = I \left| \psi_0 \right\rangle$  and  $\left| \psi^* \right\rangle = e^{s^*[\hat{H}_f, \left| \psi_0 \right\rangle \langle \psi_0 |]} \left| \psi_0 \right\rangle$ . Thus, the geodesic length on the manifold is given by

$$\|\log(e^{s^*[\hat{H}_f, \left| \psi_0 \right\rangle \langle \psi_0 |]})\|_{\text{HS}} = s^* \|\left[ \hat{H}_f, \left| \psi_0 \right\rangle \langle \psi_0 | \right]\|_{\text{HS}} = \arccos(\sqrt{E_0})/\sqrt{V_0} \cdot \sqrt{2V_0} = \sqrt{2} \arccos(\sqrt{E_0}) = \sqrt{2}d_{\text{FS}}. \quad (\text{C41})$$

Therefore, a similar result in Theorem 4 also holds for the geodesic length on the special unitary group with the bi-invariant metric.

We lastly remark that this is the optimal in the scaling in  $N$ , as mentioned in the main text. From Eq. (C34), we can further bound the left-hand side of Eq. (C28) by providing an explicit upper bound on  $s$ . Since we have

$$s^* = \frac{1}{\text{sinc}(2d_{\text{FS}})} \leq \frac{2}{|\pi/2 - d_{\text{FS}}|} = \frac{2}{\arcsin(\sqrt{E_0})} \leq \frac{2}{\sqrt{E_0}}, \quad (\text{C42})$$

we obtain

$$\frac{(2\sqrt{2}\pi)^2}{\epsilon^2} \frac{1}{\sqrt{E_0}} \leq \mathcal{N}. \quad (\text{C43})$$

We remind that  $E_0 = M/N$ . Hence, Eq. (C43) indicates that the approach also achieves the quadratic speed-up.

## 5. Proof of Theorem 5

**Theorem C.6** (Grover iteration realizes a QSP sequence). *The diffusion operator and the oracle operator in the basis  $\{|\psi_0\rangle, |\psi_0^\perp\rangle\}$  with  $|\psi_0\rangle = (1, 0)^T$  and  $|\psi_0^\perp\rangle = (0, 1)^T$  can be written as*

$$D(\alpha) = e^{i\alpha\psi_0} = e^{i\alpha/2}S_Z(\alpha/2) \quad (\text{C44})$$

$$U_f(\beta) = e^{i\beta\hat{H}_f} = e^{i\beta/2}R(\sqrt{E_0})S_Z(\beta/2)R(\sqrt{E_0}) \quad (\text{C45})$$

with  $E_0 = \langle\psi_0|\hat{H}_f|\psi_0\rangle$ , respectively. Thus, the Grover iteration can execute the  $(R(x), S_Z, |0\rangle)$ -QSP;

$$\prod_{k=1}^N G_k(\alpha_k, \beta_k) |\psi_0\rangle = S_Z(\phi_{2N}) \prod_{k=0}^{2N-1} R(\sqrt{E_0})S_Z(\phi_k) |0\rangle, \quad (\text{C46})$$

where  $\phi_0 = N\pi + \sum_{l=1}^N (\alpha_l + \beta_l)/2$ ,  $\phi_{2l-1} = \beta_l/2$  and  $\phi_{2l} = \alpha_l/2$  for  $l = 1, \dots, N$ .

*Proof.* We first verify the expression in Eq. (C46). By definition, the diffusion operator is given by

$$e^{i\alpha\psi_0} = I - (1 - e^{i\alpha})\psi_0. \quad (\text{C47})$$

Thus, by introducing

$$I = \begin{pmatrix} 1 & 0 \\ 0 & 1 \end{pmatrix}$$

and

$$\psi_0 = |\psi_0\rangle\langle\psi_0| = \begin{pmatrix} 1 & 0 \\ 0 & 0 \end{pmatrix}, \quad (\text{C48})$$

we obtain the expression

$$D(\alpha) = \begin{pmatrix} e^{i\alpha} & 0 \\ 0 & 1 \end{pmatrix}, \quad (\text{C49})$$

Similarly, we can write the oracle operator given by

$$U_f(\beta) = e^{i\beta\hat{H}_f} = I - (1 - e^{i\beta})\hat{H}_f, \quad (\text{C50})$$

in the basis. Since  $\langle\psi_0|\hat{H}_f|\psi_0\rangle = E_0$ ,  $\langle\psi_0^\perp|\hat{H}_f|\psi_0\rangle = \langle\psi_0|\hat{H}_f|\psi_0^\perp\rangle = \sqrt{E_0(1 - E_0)}$  and  $\langle\psi_0^\perp|\hat{H}_f|\psi_0^\perp\rangle = 1 - E_0$ , the matrix form of  $\hat{H}_f$  is expressed as

$$\hat{H}_f = \begin{pmatrix} E_0 & \sqrt{E_0(1 - E_0)} \\ \sqrt{E_0(1 - E_0)} & 1 - E_0 \end{pmatrix}. \quad (\text{C51})$$

Now, we decompose the matrix as

$$\begin{pmatrix} E_0 & \sqrt{E_0(1 - E_0)} \\ \sqrt{E_0(1 - E_0)} & 1 - E_0 \end{pmatrix} = \begin{pmatrix} \sqrt{E_0} & \sqrt{1 - E_0} \\ \sqrt{1 - E_0} & -\sqrt{E_0} \end{pmatrix} \begin{pmatrix} 1 & 0 \\ 0 & 0 \end{pmatrix} \begin{pmatrix} \sqrt{E_0} & \sqrt{1 - E_0} \\ \sqrt{1 - E_0} & -\sqrt{E_0} \end{pmatrix} = R(\sqrt{E_0})\psi_0R(\sqrt{E_0}), \quad (\text{C52})$$

where we use the notation defined in Eq. (C45). Here, the matrix  $R(\sqrt{E_0})$  has the property that

$$R(\sqrt{E_0})^2 = \begin{pmatrix} \sqrt{E_0} & \sqrt{1 - E_0} \\ \sqrt{1 - E_0} & -\sqrt{E_0} \end{pmatrix} \begin{pmatrix} \sqrt{E_0} & \sqrt{1 - E_0} \\ \sqrt{1 - E_0} & -\sqrt{E_0} \end{pmatrix} = \begin{pmatrix} 1 & 0 \\ 0 & 1 \end{pmatrix} = I. \quad (\text{C53})$$

Therefore, the oracle operators can be rewritten as

$$U_f(\beta) = I - (1 - e^{i\beta})\hat{H}_f = R(\sqrt{E_0})(I - (1 - e^{i\beta})\psi_0)R(\sqrt{E_0}) = R(\sqrt{E_0})D(\beta)R(\sqrt{E_0}). \quad (\text{C54})$$

Combining Eqs. (C49), (C54) together, we obtain

$$\prod_{k=1}^N G_k(\alpha_k, \beta_k) |\psi_0\rangle = (-1)^N \prod_{k=1}^N \underbrace{D(\alpha_k)}_{=e^{i\alpha_k}\psi_0} \underbrace{R(\sqrt{E_0})D(\beta_k)R(\sqrt{E_0})}_{=e^{i\beta_k}H_f} \begin{pmatrix} 1 \\ 0 \end{pmatrix}. \quad (\text{C55})$$

Now, since

$$D(\alpha) = \begin{pmatrix} e^{i\alpha} & 0 \\ 0 & 1 \end{pmatrix} = e^{i\alpha/2} \begin{pmatrix} e^{i\alpha/2} & 0 \\ 0 & e^{-i\alpha/2} \end{pmatrix} = e^{i\alpha/2} S_Z(\alpha/2), \quad (\text{C56})$$

we finally arrive at Eq. (C46).  $\square$

In this section, we also discuss how the theorem can be used to realize the ITE state. In the basis  $\{|\psi_0\rangle, |\psi_0^\perp\rangle\}$ , the ITE state can be expressed as

$$|\psi_s\rangle = \begin{pmatrix} \cos(s\sqrt{V_0}) \\ \sin(s\sqrt{V_0}) \end{pmatrix} \quad (\text{C57})$$

with  $V_0 = E_0(1 - E_0)$ . Namely, if QSP can realize the target function  $\cos(sx\sqrt{1-x^2})$ , i.e., an element in ITE state of Eq. (C57) with  $x = \sqrt{E_0}$ , the corresponding set of angles can be used for realizing the ITE state via the Grover iterations.

As discussed in App. B4, the function must satisfy five conditions for successful realization via QSP in this setting. The first three conditions are straightforwardly satisfied; the cosine function  $\cos(t)$  is an even function, bounded by 1 for  $t \in [-1, 1]$ , and can be approximated by degree- $K$  polynomials using e.g., Taylor expansion. In general, the fourth and fifth conditions significantly restrict the class of realizable functions [19]. Despite this, the target function meets both conditions favorably. For the fourth condition, observe that  $\sqrt{1-x^2} \in \mathbb{C}$  for  $x \in (-\infty, -1] \cup [1, \infty)$ , and since  $\cos(it) = \cosh(t)$ , the function  $\cos(sx\sqrt{1-x^2})$  exceeds 1 in magnitude, as required. For the fifth condition, note that the function is even. To verify this condition, we evaluate the function under the substitution  $x \rightarrow ix$  and then we have  $\cos(isx\sqrt{1+x^2}) = \cosh(sx\sqrt{1+x^2})$ , which is real and greater than 1 for  $x \in \mathbb{R}$ ; that is the requirement is satisfied. As a result, all five conditions are met, and thus there exists a set of QSP angles that realizes the target function for sufficiently large polynomial degrees.

We further consider the QSP implementation of ITE for unstructured search. Theorem 5 establishes the existence of a set of angles that enables QSP implementation of ITE for a large value of  $N$ . However, it does not provide insights into the efficiency and feasibility of the implementation. Indeed, it is known that trigonometric functions admit a low-degree polynomial approximation:

**Lemma C.7** (Polynomial approximation of trigonometric functions by Jacobi-Anger expansion [18, 19]). *Consider  $s \in \mathbb{R}$  and  $\epsilon \in (0, \frac{1}{e})$ . Let  $K = \lfloor \frac{1}{2}r(s, \epsilon) \left( \frac{e|s|}{2}, \frac{5}{4}\epsilon \right) \rfloor$  be a degree. Then, trigonometric functions can be approximated as follows;*

$$\|\cos(sx) - J_0(s) + 2 \sum_{l=1}^K (-1)^l J_{2l}(s) T_{2l}(x)\|_{[-1,1]} \leq \epsilon, \quad (\text{C58})$$

$$\|\sin(sx) - 2 \sum_{l=1}^K (-1)^l J_{2l+1}(s) T_{2l+1}(x)\|_{[-1,1]} \leq \epsilon, \quad (\text{C59})$$

where  $T_m(x)$  are the Chebyshev polynomials of the first kind,  $J_m(s)$  are the Bessel functions of the first kind and  $r(s, \epsilon)$  is a function that asymptotically scales as

$$r(s, \epsilon) = \Theta \left( |s| + \frac{\log(1/\epsilon)}{\log(e + \frac{\log(1/\epsilon)}{|s|})} \right). \quad (\text{C60})$$

This suggests that trigonometric functions can be approximated using Chebyshev polynomials of degree  $K = \lfloor \frac{1}{2}r(s, \epsilon) \left( \frac{e|s|}{2}, \frac{5}{4}\epsilon \right) \rfloor$  with the error  $\epsilon$ . However, there is a caveat; the target function in our case is  $\cos(sg(x))$  with  $g(x) =$

$x\sqrt{1-x^2}$ , which introduces additional nonlinearity. As a result, a higher polynomial degree may be required to achieve the same approximation accuracy. Nevertheless, it does not incur significant additional cost. Suppose  $\cos(x)$  can be approximated by a polynomial of degree  $2K$ , i.e.,  $\cos(x) \approx \sum_{l=1}^K c_l x^{2l}$  with a specific coefficient set  $\{c_l\}$ . Now, by replacing  $x$  with  $g(x) = x\sqrt{1-x^2}$ , the approximation of  $\cos(g(x))$  is given by

$$\cos(g(x)) \approx \sum_{l=1}^K c_l (x\sqrt{1-x^2})^{2l} = \sum_{l=1}^K c_l (x^2(1-x^2))^l = \sum_{l=1}^K c'_l x^{4l} \quad (\text{C61})$$

with the set of rearranged coefficients  $\{c'_l\}$ . Therefore, the degree required to realize  $\cos(g(x))$  is still  $4K$ , indicating the complexity is the same as  $\cos(x)$  up to the multiplicative factor 2.

Next, we show that the solution state  $|\psi^*\rangle$  can be approximately realized using this QSP formulation of ITE for unstructured search. Here, given the Grover iteration  $\prod_{k=1}^N G_k(\alpha_k, \beta_k)$ , we aim to realize  $W|\psi_0\rangle = |\psi_0\rangle$ , where the matrix  $W$  is defined as

$$W \equiv D(\beta_N)R(\sqrt{E_0}) \prod_{k=1}^{N-1} G_k(\alpha_k, \beta_k), \quad (\text{C62})$$

by properly choosing  $\{(\alpha_k, \beta_k)\}_{k=1}^N / \{\alpha_N\}$  via QSP. Namely, if we can realize  $W|\psi_0\rangle = |\psi_0\rangle$ , we obtain

$$\begin{aligned} (-1) \prod_{k=1}^N G_k(\alpha_k, \beta_k) |\psi_0\rangle &= D(0)R(\sqrt{E_0})W|\psi_0\rangle \\ &= \begin{pmatrix} \sqrt{E_0} & \sqrt{E_0(1-E_0)} \\ \sqrt{E_0(1-E_0)} & -\sqrt{E_0} \end{pmatrix} \begin{pmatrix} 1 & 0 \\ 0 & \pm 1 \end{pmatrix} \begin{pmatrix} 1 \\ 0 \end{pmatrix} \\ &= \begin{pmatrix} \sqrt{E_0} \\ \sqrt{E_0(1-E_0)} \end{pmatrix} = |\psi^*\rangle, \end{aligned} \quad (\text{C63})$$

by setting  $\alpha_N = 0$ . That is, since a simple application of  $R(\sqrt{E_0})$  to the initial state prepares the solution state  $|\psi^*\rangle = (\sqrt{E_0}, \sqrt{1-E_0})^T$ , we aim to realize  $\langle\psi_0|W|\psi_0\rangle = 1$

An example of the target function to realize Eq. (C62) via QSP would be the sign function. Note that we require  $p_{QSP}(\sqrt{E_0}) = \langle 0|W|0\rangle = 1$ , but we do not care about the value of  $p_{QSP}(x)$  for negative  $x$  values as  $\sqrt{E_0}$  is always positive. From this perspective, a constant function can also satisfy the condition. However,  $W$  is composed of an odd  $(2N-1)$  number of applications of the signal operator  $R(\sqrt{E_0})$ , meaning the function is necessarily an odd function. Thus, implementing the sign function by obtaining the set of angles  $\{(\alpha_k, \beta_k)\}_{k=1}^N / \{\alpha_N\}$  can realize the fixed-point algorithm, since the QSP formulation does not require information on  $\sqrt{E_0}$ . Note that, the solution state can be obtained by applying  $R(\sqrt{E_0})$  to the initial state  $|\psi_0\rangle$ , i.e.,  $|\psi^*\rangle = R(\sqrt{E_0})|\psi_0\rangle$  by definition. However, the Grover iteration inherently applies an even number of  $R(\sqrt{E_0})$  and thus cannot implement a single  $R(\sqrt{E_0})$ . Therefore, we construct the matrix Eq. (C62) to realize the solution state.

We begin by analyzing how the approximation error in the target function, introduced through the QSP construction, propagates to the final fidelity, defined as  $F = |\langle\psi^*|\tilde{\psi}\rangle|^2$ , where  $|\tilde{\psi}\rangle$  is the final state obtained from the QSP formulation of ITE. Assume that the QSP approximation incurs an error of  $\delta^2/2$  and hence the matrix  $W$  in Eq. (C62) can be changed such that

$$\tilde{W} = \begin{pmatrix} 1 - \delta^2/2 & * \\ * & * \end{pmatrix}. \quad (\text{C64})$$

Then, the fidelity is given by

$$\begin{aligned} |\langle\psi^*|(-1)D(0)R(\sqrt{E_0})\tilde{W}|\psi_0\rangle|^2 &= \left| \begin{pmatrix} \sqrt{E_0} & \sqrt{1-E_0} \\ \sqrt{1-E_0} & -\sqrt{E_0} \end{pmatrix} \begin{pmatrix} 1 - \delta^2/2 & * \\ * & * \end{pmatrix} \begin{pmatrix} 1 \\ 0 \end{pmatrix} \right|^2 \\ &= \left| \begin{pmatrix} 1, 0 \\ * & * \end{pmatrix} \begin{pmatrix} 1 - \delta^2/2 & * \\ * & * \end{pmatrix} \begin{pmatrix} 1 \\ 0 \end{pmatrix} \right|^2 \\ &= (1 - \delta^2/2)^2 \geq 1 - \delta^2, \end{aligned} \quad (\text{C65})$$

with  $\alpha_N = 0$ . Thus, if the approximation to the sign function is sufficiently accurate, the final state remains close to the desired solution state.

The remaining question concerns the polynomial degree required to attain the desired precision. Actually, there exists an effective approximation technique for the function:

**Lemma C.8** (Approximation of the sign function  $\text{sgn}(x)$  [19, 78]). *Consider  $\eta > 0$ ,  $x \in \mathbb{R}$  and  $\Delta \in (0, 1/2)$ . Given a degree  $K = \mathcal{O}(\log(1/\Delta)/\eta)$ , there exists an odd polynomial  $p(x)$ , such that*

- for all  $x \in [-2, 2]$ :  $|p(x)| \leq 1$  and
- for all  $x \in [-2, 2] \setminus (-\eta, \eta)$ :  $|p(x) - \text{sgn}(x)| \leq \Delta$

where

$$\text{sgn}(x) = \begin{cases} 1 & \text{if } x > 0, \\ -1 & \text{if } x < 0, \\ 0 & \text{if } x = 0. \end{cases} \quad (\text{C66})$$

Consequently, combining the error analysis in Eq. (C65) with the parameters  $\eta = \sqrt{E_0}$  and  $\Delta = \delta^2/2$  reveals that a degree of polynomial  $K \in \mathcal{O}(\log(2/\delta^2)/\sqrt{E_0})$  ensures that the final fidelity exceeds  $1 - \delta^2$ . This scaling matches the complexity of the fixed-point algorithm.

We note that the sign function does not satisfy the conditions for the achievable functions via the  $(R(x), S_Z, |0\rangle)$ -QSP setting, as shown in App. B 4. However, Ref. [19] demonstrates that, allowing for a small imaginary components enables the effective approximation of the sign function in practical settings. Therefore, while additional errors may occur because of the imaginary components, the implementation can be feasible in practice.

## Appendix D: Numerical Simulations

In this section, we perform numerical simulations to verify the QSP formulation of ITE for unstructured search. Specifically, we examine two aspects: (1) the accuracy of the approximation for realizing ITE and (2) the performance of the fixed-point algorithm using the approximated sign function, in comparison with existing methods.

First, we numerically demonstrate that the ITE state in Eq. (C57) can be realized by properly choosing  $\boldsymbol{\alpha} = \{\alpha_k\}_{k=1}^{2N}$  in

$$U(\boldsymbol{\alpha}, x) = \prod_{k=1}^{2N} D(\alpha_k) R(x) = \prod_{k=1}^{2N} \begin{pmatrix} e^{i\alpha_k} & 0 \\ 0 & 1 \end{pmatrix} \begin{pmatrix} x & \sqrt{1-x^2} \\ \sqrt{1-x^2} & -x \end{pmatrix}, \quad (\text{D1})$$

via the QSP implementation of  $p(x) = \cos(sx\sqrt{1-x^2})$ . In the numerical simulation, we heuristically optimize  $\boldsymbol{\alpha}$  such that  $\text{Re}(\langle 0|U(\boldsymbol{\alpha}, x)|0\rangle) \approx p(x)$ ,  $x \in [0, 1]$ . Here,  $|0\rangle = (1, 0)^T$  corresponds to the initial state  $|\psi_0\rangle$  and  $|1\rangle = (0, 1)^T$  corresponds to  $|\psi_0^\perp\rangle$  for the ITE formulation. We recall that the input domain is restricted to  $[0, 1]$ , since  $E_0$  only takes a non-negative value for unstructured search. To perform the optimization, we introduce the following cost function;

$$\mathcal{L}(\boldsymbol{\alpha}) = \frac{1}{n_d} \sum_{i=1}^{n_d} (p(x_i) - \text{Re}(\langle 0|U(\boldsymbol{\alpha}, x_i)|0\rangle))^2 + \lambda_1 \frac{1}{n_d} \sum_{i=1}^{n_d} \text{Im}(\langle 0|U(\boldsymbol{\alpha}, x_i)|0\rangle)^2 + \lambda_2 \frac{1}{n_d} \sum_{i=1}^{n_d} \arg\left(\frac{\langle 0|U(\boldsymbol{\alpha}, x_i)|0\rangle}{\langle 1|U(\boldsymbol{\alpha}, x_i)|0\rangle}\right)^2, \quad (\text{D2})$$

where the first term represents the mean square errors between the approximated and the target functions, while the remaining two terms are introduced as the penalty with the coefficients  $\lambda_1$  and  $\lambda_2$ . Concretely, the second term penalizes the imaginary part of  $\langle 0|U(\boldsymbol{\alpha})|0\rangle$  to make it zero. The third term suppresses the relative phase between  $\langle 0|U(\boldsymbol{\alpha}, x)|0\rangle$  and  $\langle 1|U(\boldsymbol{\alpha}, x)|0\rangle$ , which is necessary because the resulting state after applying  $U(\boldsymbol{\alpha})$  is

$$U(\boldsymbol{\alpha}, x)|0\rangle = \begin{pmatrix} \langle 0|U(\boldsymbol{\alpha}, x)|0\rangle \\ \langle 1|U(\boldsymbol{\alpha}, x)|0\rangle \end{pmatrix}, \quad (\text{D3})$$

and we aim to approximate  $(\cos(sx\sqrt{1-x^2}), \sin(sx\sqrt{1-x^2}))^T$  for an arbitrary  $s \geq 0$  up to a global phase with this; that is, the relative phase is distinguishable and hence incurs the additional errors when implementing ITE with the phase obtained through the QSP construction. In the following simulation, we employ the “scipy.optimize.minimize” function from SciPy [79], using the Sequential Least Squares Programming (SLSQP) method. The penalty coefficients are set  $(\lambda_1, \lambda_2) = (0.01, 0.1)$ , and we use  $n_d = 50$  samples, uniformly drawn from the interval  $[0, 1]$ .

Fig. 4 (a) shows the infidelity between the ITE state in Eq. (7) and the state  $U(\boldsymbol{\alpha}, x)|\psi_0\rangle$  with a set of angles obtained via the optimization for  $N = 16$ ,  $s = 0.5, 1, 3$  and  $N = 2^8$ . The infidelity is defined as  $\mathcal{I} = 1 - |\langle \psi_s|U(\boldsymbol{\alpha}, x)|\psi_0\rangle|^2$ , where  $|\psi_s\rangle$  is the ITE state in Eq. (7). We observe that the Grover iteration using the optimized QSP angles can accurately reproduce the ITE state. The difference in accuracy with respect to the initial overlap  $E_0$  can be attributed to numerical optimization error. More specifically, while the target function is realized by  $\langle 0|U(\boldsymbol{\alpha}, x)|0\rangle$  effectively, the numerical optimization does not fully eliminate

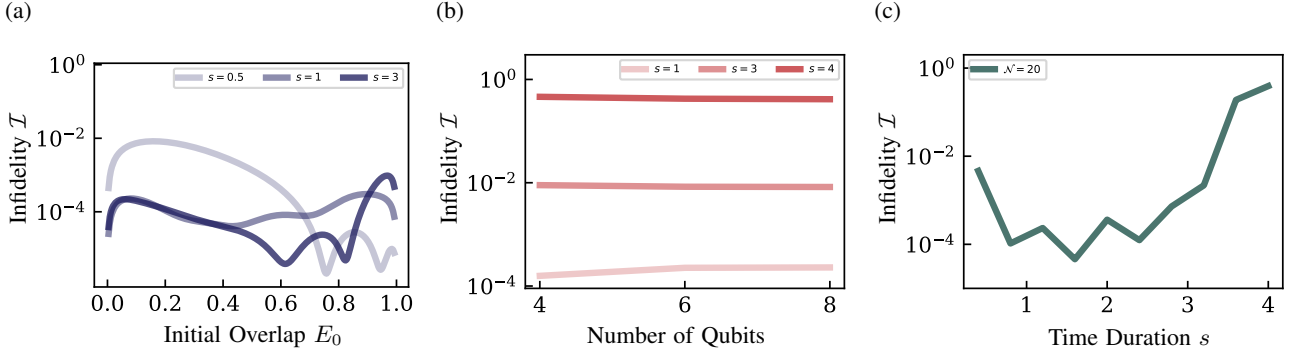


FIG. 4. **Numerical simulations of QSP formulation for ITE.** We numerically verify the QSP formulation of ITE for unstructured search. (a) Using the set of angles derived from the QSP formulation, we compute the infidelity between the ITE state defined in Eq. (7) and the state obtained after applying the Grover iteration with  $\mathcal{N} = 16$  to the initial state for  $N = 2^8$ . Across the entire range of initial overlaps  $E_0$ , the infidelity remains below  $10^{-2}$  for  $s = 0.5, 1$ , and  $3$ . (b) We check the dependence on the system size  $N = 2^n$  with  $n = 4, 6, 8$  for  $s = 1, 3, 4$ . As shown in Theorem 5, the performance does not depend on the system size. (c) We further check the dependence of performance on the time duration. Using  $\mathcal{N} = 20$  for the Hamiltonian  $\hat{H}_f$  of size  $N = 2^6$ , we confirm that the large value of  $s$  incurs more errors, as indicated by Lemma C.7.

the relative phase error, i.e.,  $\arg\left(\frac{\langle 0|U(\alpha, x_i)|0\rangle}{\langle 1|U(\alpha, x_i)|0\rangle}\right) \neq 0$ . Consequently, we have an input-dependent difference caused by a nonzero, input-dependent relative phase.

We then check the system-size dependence by using the Hamiltonian  $\hat{H}_f$  of the size  $N = 2^n$  with  $n = 4, 6, 8$  for  $s = 1, 3, 4$ . The number of Grover iterations is set as  $\mathcal{N} = 8$  and we compute the infidelity averaged over the choice of the number of targets  $M = 1, \dots, 2^n - 1$ . As shown in Fig. 4 (b), we confirm that the approximation error remains independent of the system size. This behavior is consistent with Theorem 5, which establishes the equivalence between the ITE state and its two-dimensional representation. We also note that a large value of the time duration  $s$  incurs a big error, which motivates the following numerical experiments.

We also examine the dependence of performance on the time duration  $s$ . Here, we consider  $\hat{H}_f$  of the size  $N = 2^6 = 64$  and the number of queries  $\mathcal{N} = 20$ . According to Lemma C.7, the polynomial degree required to approximate the target trigonometric functions grows linearly with the time duration. In agreement with this theoretical expectation, Fig. 4 (c) shows that the Grover iteration with a fixed number of polynomial degree fail to realize the ITE state for larger values of  $s$ . Note that the case with  $s < 1$  exhibits higher infidelity compared to the cases with  $1 \leq s \leq 3$ . However, since the infidelity remains below 0.01 in all cases, the observed deviation can be attributed to optimization error rather than fundamental limitations. Overall, the numerical results verify that the ITE state in Eq. (7) can be effectively reconstructed using the QSP formulation.

Next, we benchmark the performance of our QSP formulation of ITE for a fixed-point search by comparing it with the original Grover and fixed-point algorithms. The set of angles for each algorithm is as follows;

- **Standard Grover method:** The phase angles for the original work [1] is given by

$$\alpha_k = \beta_k = \pi. \quad (\text{D4})$$

- **Original fixed-point angles:** In the original fixed-point algorithm [16], the phase angles are given by

$$\alpha_k = \beta_{N-k+1} = -\cot^{-1}\left(\tan\left(\frac{2\pi k}{N}\right)\sqrt{1 - \frac{1}{\gamma^2}}\right), \quad (\text{D5})$$

where  $\gamma = T_{1/\mathcal{N}}(1/\delta)$  is the Chebyshev polynomial of the first kind and we set the target infidelity  $\delta^2 = 0.1$ .

- **Our proposal:** We use the heuristic approach mentioned above to derive phase angles for a polynomial function that approximates the sign function, such that  $W|0\rangle = |0\rangle$ . We also set  $\alpha_{2\mathcal{N}} = 0$  to realize the solution state  $|\psi^*\rangle$ .

Fig. 5 (a) illustrates the fidelity between the solution state and the output state generated by Grover iterations,  $F = |\langle\psi^*|\tilde{\psi}\rangle|^2$ , where  $|\tilde{\psi}\rangle$  is a state generated by Grover iterations with  $\mathcal{N} = 20$  using the three different sets of phase angles. In this simulation,

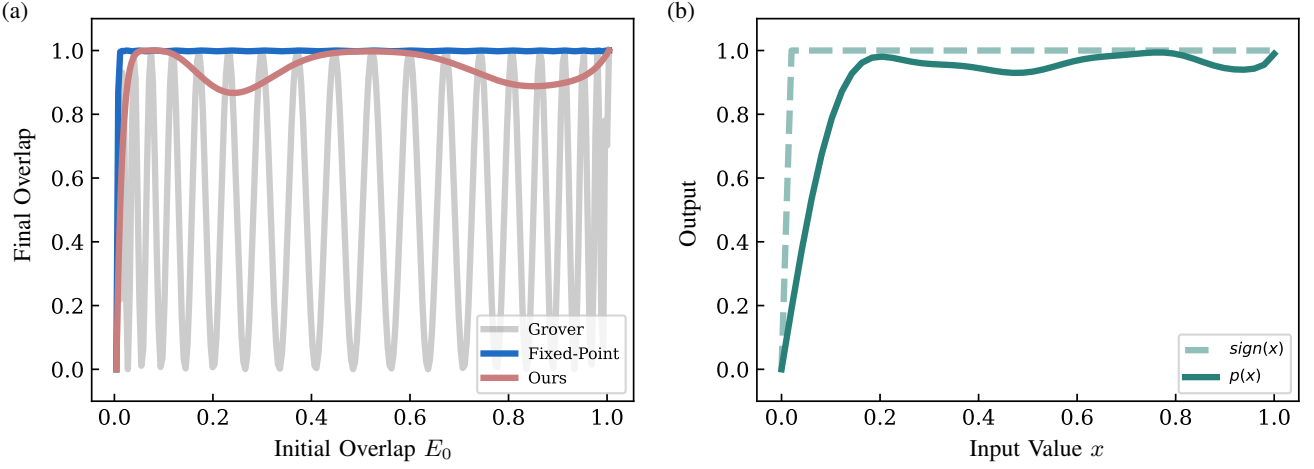


**FIG. 5. Comparison of our proposal to the original Grover algorithm and fixed-point algorithm.** We compare the performance of our proposed method with the original Grover and fixed-point algorithms. (a) We demonstrate the overlap after employing these algorithms against the initial overlap  $E_0$ . In this comparison, we fix  $\mathcal{N} = 20$  and consider a Hamiltonian of dimension  $2^8$ , where the number of target items  $M$  is varied according to the initial overlap  $E_0 = M/N$ . (b) The approximated sign function  $p(x)$  obtained via heuristic optimization is illustrated. While the results in (a) exhibit slightly lower performance than the original fixed-point algorithm due to optimization error, the proposed method successfully mitigates overshooting.

we set  $n = 8$ , which corresponds to a search space of  $2^8 = 256$  items, and consider  $M = 0, 1, \dots, N$  so that we check the performance depending on  $E_0 = M/N$ . As for the fixed-point algorithm, we set  $\delta^2 = 0.1$ . The results show that our method achieves fidelity comparable to that of the fixed-point algorithm, while avoiding the overshooting behavior exhibited by the original Grover algorithm. The minor discrepancy in performance can be attributed to the approximation error in the sign function used in the QSP construction. Fig. 5 (b) shows the approximated function realized via the QSP procedure, along with the associated approximation error. Despite this small error, our approach remains highly effective and closely matches the performance of the fixed-point method. These results validate the practical effectiveness of our QSP formulation and provide new insights into the design of the fixed-point algorithm.